Design of Prestressed, Fabric-Formed Concrete Beams

By
Nicolas Gomez

B.S. Civil Engineering
Massachusetts Institute of Technology, 2016

SUBMITTED TO THE DEPARTMENT OF CIVIL AND ENVIRONMENTAL ENGINEERING IN PARTIAL FULFILLMENT OF THE REQUIRMENTS FOR THE DEGREE OF

MASTER OF ENGINEERING IN CIVIL AND ENVIRONMENTAL ENGINEERING

at the

MASSACHUSETTS INSTITUTE OF TECHNOLOGY

June 2017

Signature of Author: Signature redacted
Department of Civil and Environmental Engineering
May 12, 2017

Certified by: Signature redacted
John A. Ochsendorf
Class of 1942 Professor of Civil and Environmental Engineering and Architecture

Accepted by: Signature redacted
Jesse Kroll
Associate Professor of Civil and Environmental Engineering
Chair, Departmental Committee for Graduate Students

Design of Prestressed, Fabric Formed Concrete Beams

By

Nicolas Gomez

Submitted to the Department of Civil an Environmental Engineering on May 12th, 2017 in Partial Fulfillment of the Requirements for the Degree of Master of Engineering in Civil and Environmental Engineering.

Abstract

Fabric forms and prestressing are both technologies for concrete structures that allow for less material to do more work. This thesis seeks to assess the feasibility and performance of fabric formed, prestressed beams with a keyhole cross-section, while varying parameters such as concrete strength, loading, beam depth, and prestressing force. They are designed for flexure via a sectional method, starting with the critical midspan section, and each section is iterated in an effort to minimize the beam weight. Beam strength and deflections are determined and once met, they are compared to more traditional prestress designs. Such beams are found to be governed primarily by strength criteria, as deflections are found to be minimal. These fabric formed beams can use nearly an identical amount of material as conventional I-beams with a constant cross-section, while requiring a higher prestressing force. Prestressed fabric formed beams are less efficient than an I-beam section, but should not be discounted as a viable element, because of their aesthetic appeal and further potential for optimization.

Acknowledgements

I'd like to thank the multitude of people who made it possible for me to pursue my degree and this topic. The first being Professor Mark West, who introduced me to fabric forms this year, and was incredibly understanding as I bumbled through my first architecture workshop and exposed me to an architect's thought process. And to Professor John Ochsendorf for his patience and guidance in the production of this work. I would also like to thank Professor Tim Ibell and Dr. John Orr, for their brief but helpful communications in starting this work.

And to those supported me outside my academic work. My peers, Momo Sun and Anthony McHugh, I cannot understate the degree your friendships enabled me to push through late nights. And lastly to my parents, Andres and Lelia Gomez, who without their lives of sacrifice, I would not be here at MIT, much less completing this thesis.

Table of Contents

Table of Figures

Symbols and Notations

$A_c = area\ of\ concrete\ cross\ section$

$w_{conc} = density\ of\ concrete\ in\ lbs\ per\ cubic\ foot$

$E_c = Modulus\ of\ Elasticity\ of\ concrete$

$e = eccentricity\ of\ prestress\ tendon\ from\ center\ of\ gravity$

$P_i = initial\ prestress\ force\ of\ tendon$

$P_e = eventual\ prestress\ force\ of\ tendon\ after\ losses$

$\gamma = prestress\ loss\ ratio$

$y = vertical\ coordinate\ of\ beam\ cross - section$

$L = length\ of\ span$

$I_{xx} = Second\ moment\ of\ inertia$

$f'_c = concrete\ compressive\ strength$

$f'_{ci} = initial\ concrete\ compressive\ strength$

$f_{ci} = initial\ allowable\ concrete\ compressive\ stress$

$f_{ti} = initial\ allowable\ concrete\ tensile\ stress$

$f_c = long - term\ allowable\ concrete\ compressive\ stress$

$f_t = long - term\ allowable\ concrete\ tensile\ stress$

$h_1 = depth\ of\ beam\ at\ midspan$

$h_2 = thickness\ of\ top\ flange$

$h = depth\ of\ beam\ at\ section$

$b_{flange} = width\ of\ flange$

$b_{web} = width\ of\ web$

$r_{chord} = radius\ of\ bottom\ chord\ for\ beam$

$y_{c.g.} = distance\ to\ center\ of\ gravity\ measured\ from\ top\ of\ beam$

S^t = *Section Modulus with respect to the top fiber*

S_b = *Section modulus with respect to the bottom fiber*

c^t = *distance from top fiber to center of gravity*

c_b = *distance from bottom fiber to center of gravity*

q_L = *line load from live oad*

M_{SW} = *moment due to self − weight*

M_{DL} = *moment due to dead load*

M_{LL} = *Moment due to live load*

V_c = *Shear capacity f section*

V_c = *vertical component of prestress at section*

1. Introduction

This thesis tackles the feasibility and potential efficiency of combining two technologies: prestressed reinforcement and fabric forms. The essence of each technology is introduced and then several beams with various parameters are analytically modeled and assessed.

This thesis asks two questions. Is there potential for fabric-formed, prestressed beams to be used in current practice, such that they meet the requisite strength and serviceability criteria. Such a beam should be reasonably designed, so that an appropriate prestressing force, amount of material, and conceivable construction process is used.

Both fabric forms and prestressing allow designers to increase the material efficiency of their structure. A combination of these two technologies would have some initial hurdles before it could be used in common practice. As such, this thesis also seeks to answer whether there are significant enough material savings to warrant a push to introduce fabric formed, prestressed beams into practice.

1.1 Motivation

The primary motivation of this work is to expand engineering knowledge of fabric formed, prestressed beams in order to further support the industry drive for greater material efficiency and sustainability. The construction industry accounts for a significant part of global emissions, and cement manufacturing alone comprises 5% of all global emissions by humanity (World Business Council for Sustainable Development, 2002). A great impact can be made by moving away from the standard of prismatic sections. And beyond the rote economics of efficiency and cost, fabric forms are architecturally more appealing, as they are an expression of form flowing from forces (West, 2017).

1.2 Fabric Formwork

Concrete has a unique property in being a liquid before it is set and can potentially take any shape, but either for ease of constructability, ease of design, or both, it is often forced to take a rectangular prismatic shape. Pier Luigi Nervi once said, "Until these bonds are totally removed, the architecture of concrete structures is bound to be ... an architecture of wooden planks" (West, 2017 p.44). Today however, with increasing power of computation and the cumulative work of researchers, it has become possible to economically create and analyze more complex forms that are more aesthetically pleasing and efficient than conventional cuboid shapes.

Fabric forms offer one such way to do this, allowing concrete to express its form through the force flows (West, 2017). The beam in Figure 1.1 for example, is designed to be a more material efficient element to support a uniform loading. The beam resembles the moment diagram for such a loading, and by simply utilizing a more efficient shape, up to 60% of the concrete material could be saved (Orr, 2012). Part of the allure of fabric forms is the relative ease with which an elegant structure can be created. Previously, to create the kind of form seen Figure 1.1, it may have taken a series of carved foam blocks or a series of assembled plywood sheets to create the negative mold required. With an appropriate sheet fabric and the right anchorage points, the beam can be cast in fabric with much less effort. And unlike with a foam or wood mold, the fabric and framework can be dissembled and reused without the destruction of the mold.

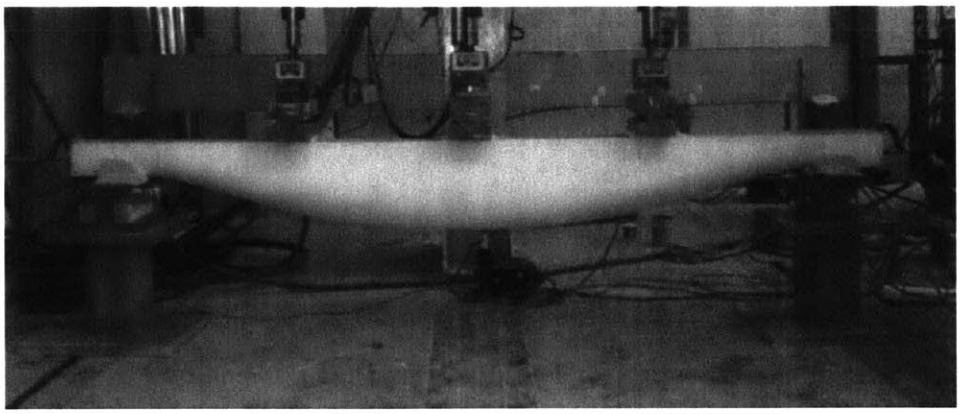

Figure 1.1: Photo from Garbett et al. (2010) of three point test for fabric formed beam.

1.3 Purpose

The purpose of this work is to explore the feasibility and potential efficiency for a prestressed fabric formed concrete beam. Beams are designed under varying parameters (concrete strength, loading bay size, constrained span/depth ratio, etc.) and assessed for strength and deflection limits.

1.4 Outline

Chapter 2 will review current literature and the state of research in fabric forms, as well as a quick review of the principles of prestressing. Chapter 3 will outline the methodologies and calculations used to design the beams. Chapter 4 will portray and interpret results. Chapter 5 will conclude the thesis, summarize findings, and outline potential future work on this topic.

2. Literature Review

2.1 Fabric Forms

2.1.1 Architectural Expression and CAST

Fabric formwork has been in use since at least 1899, when Gustav Lilienthal filed a patent for a fabric formed suspended floor (Veenendaal et al., 2011b). Since then however, it has burgeoned into a developed field with many prominent researchers, exploring the technology for various reasons.

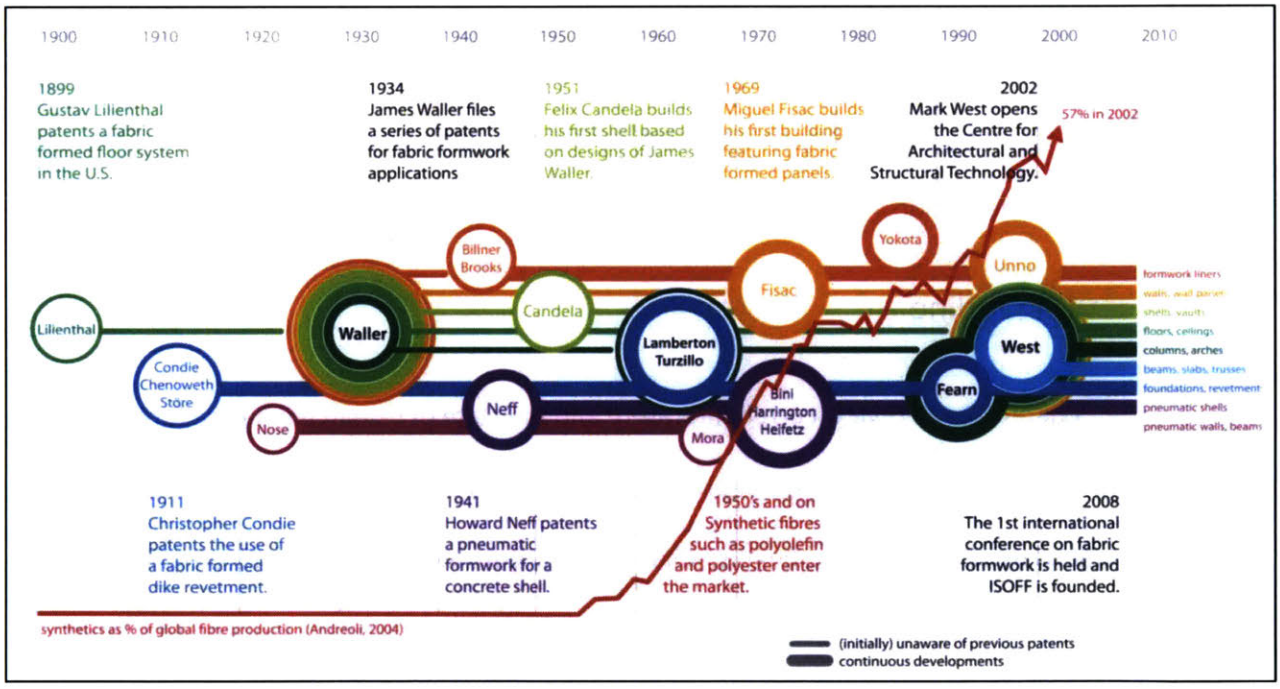

Figure 2.1: Diagram from Veenendaal et al. (2011b) outlining the history of fabric formwork.

The field has seen a recent growth in interest and innovation, partly due to the foundation of the Center for Architectural Structures and Technology (CAST) in Manitoba University in 1990's. Their work, largely lead by Mark West, has explored the use of flexible

forms in both architectural and technical aspects (West, 2017). One of their major contributions is in developing construction techniques for unique structures, tackling the complex constraints arising from the shape and the nature of fabric forms. One example method for creating a fabric formed beam cast is to have two suspended platforms, with a cloth hung between the two. Figure 2.2 shows an example of this, with the fabric draped and held in place with wooden anchors, along with the passive steel reinforcement suspended above the fabric.

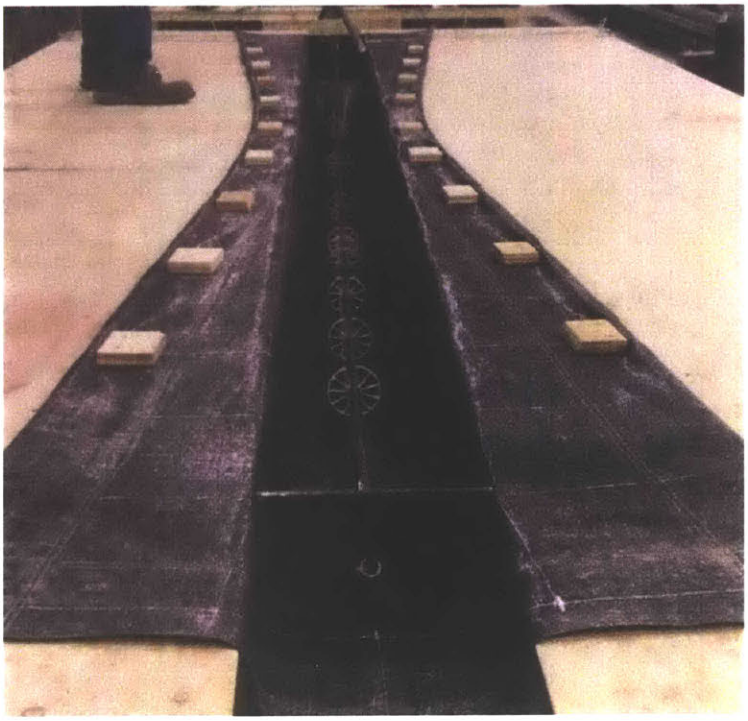

Figure 2.2 Photo from West (2017) of fabric formwork with reinforcement before the pour

In exploring various forms and techniques, CAST and West have demonstrated numerous advantages of fabric forms. Beyond the potential for organic forms that support material efficiency, the permeable membrane allows for the concrete to cure more uniformly. Air bubbles and excess water can exit the element through the membrane rather than just the

exposed concrete surface like in normal casts. This allows for a higher quality finish free of pock marks. As well, the lightweight nature of the formwork allows for versatility in set up and ease of transportation.

2.1.2 Engineering Fabric Formed Structures

Beyond the architectural aspirations, others have sought to quantify the behavior and design of fabric forms. One primary goal is to predict the behavior of the concrete elements once cast as well as optimizing their design to use the fabric form and the element to their full potential.

Orr (2012) explores three aspects of fabric formed beams with passive reinforcement. This includes structural behavior, durability, and methods required to design and build the beams. To this end, he investigated several potential cross section types: including fish belly beams, T-beams, and double-keel T-beams shown in Figure 2.3.

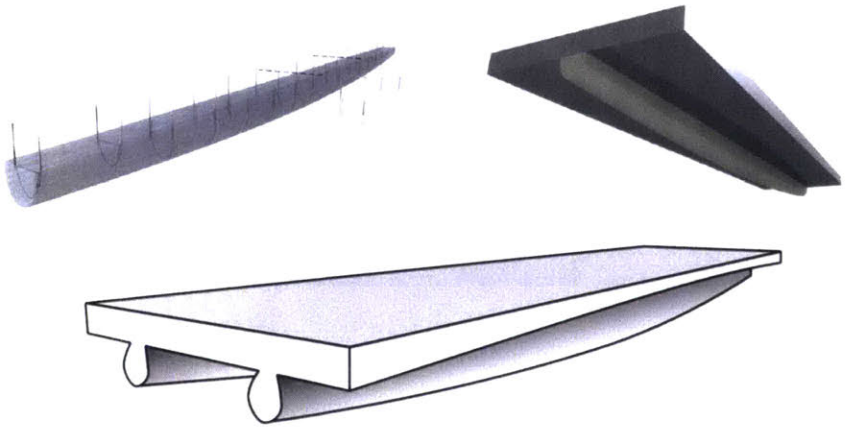

Figure 2.3: Selected beams from Orr (2012)

Another large component was conceptualizing the detailing and construction process for creating such beams. Orr (2012) details a collaborative work experience with West, during

an extended stay at the University of Manitoba. Together, they worked on the construction process and developing different forms of beams, casting several prototypes at CAST.

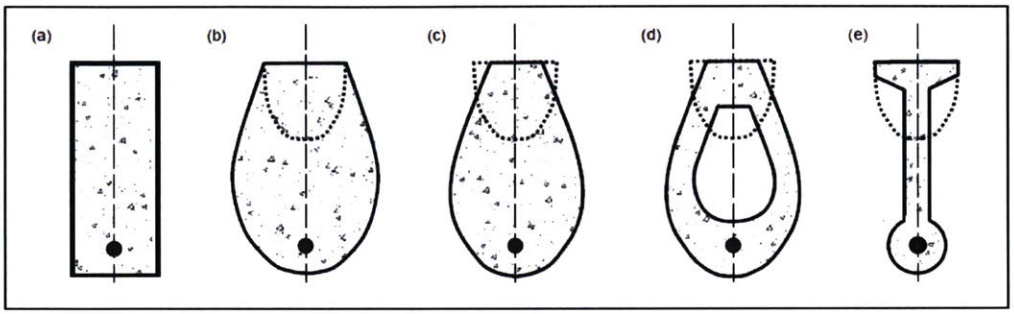

Figure 2.4: Various Cross-sections for fabric forms from Garbett et al. (2010)

Figure 2.4 shows various potential cross sections analyzed, compared against a traditional prismatic beam. Figure 2.4(b) and (c) show a 'fish belly' type beam that is simplest to make via the method shown in Figure 2.2. Figure 2.4(e) shows a 'keyhole' design, similar to an I-beam, which would increase the moment of inertia while reducing total material used. This thesis will focus on using such a beam as the basis for a prestressed design, as it is the most similar to existing prestressed cross-sections. Figure 2.5 shows the framework used in Garbett et al. (2010) for forming the straight web in a fabric form, where flat sheet were used to constrain the expansion of the fabric.

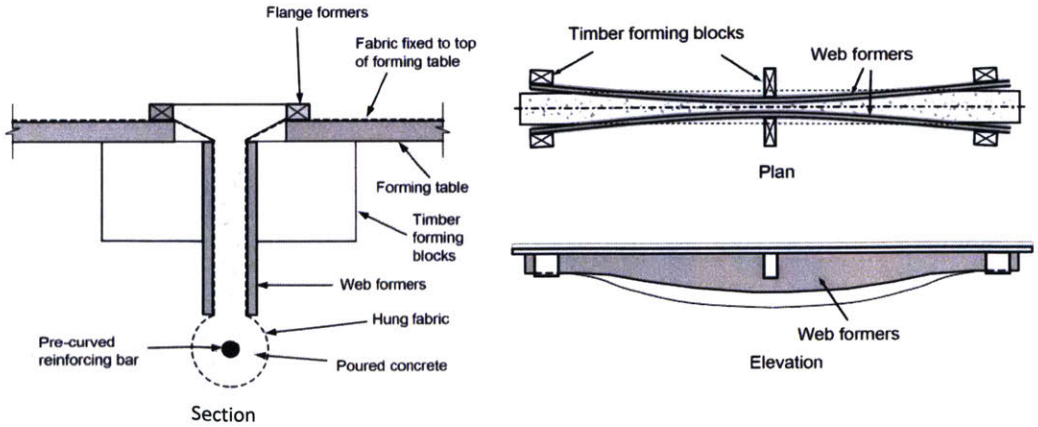

Figure 2.5: Section, Plan, and Elevation view of formwork for keyhole type beam, taken from Garbett et al. (2010)

Garbett et al. (2010) and Orr (2012) each describe a general design process for creating passively reinforced beams shown below. They begin with the initial loading and support conditions, and create a beam geometry and assess its performance for several points along the length of the beam, as outlined in Figure 2.6.

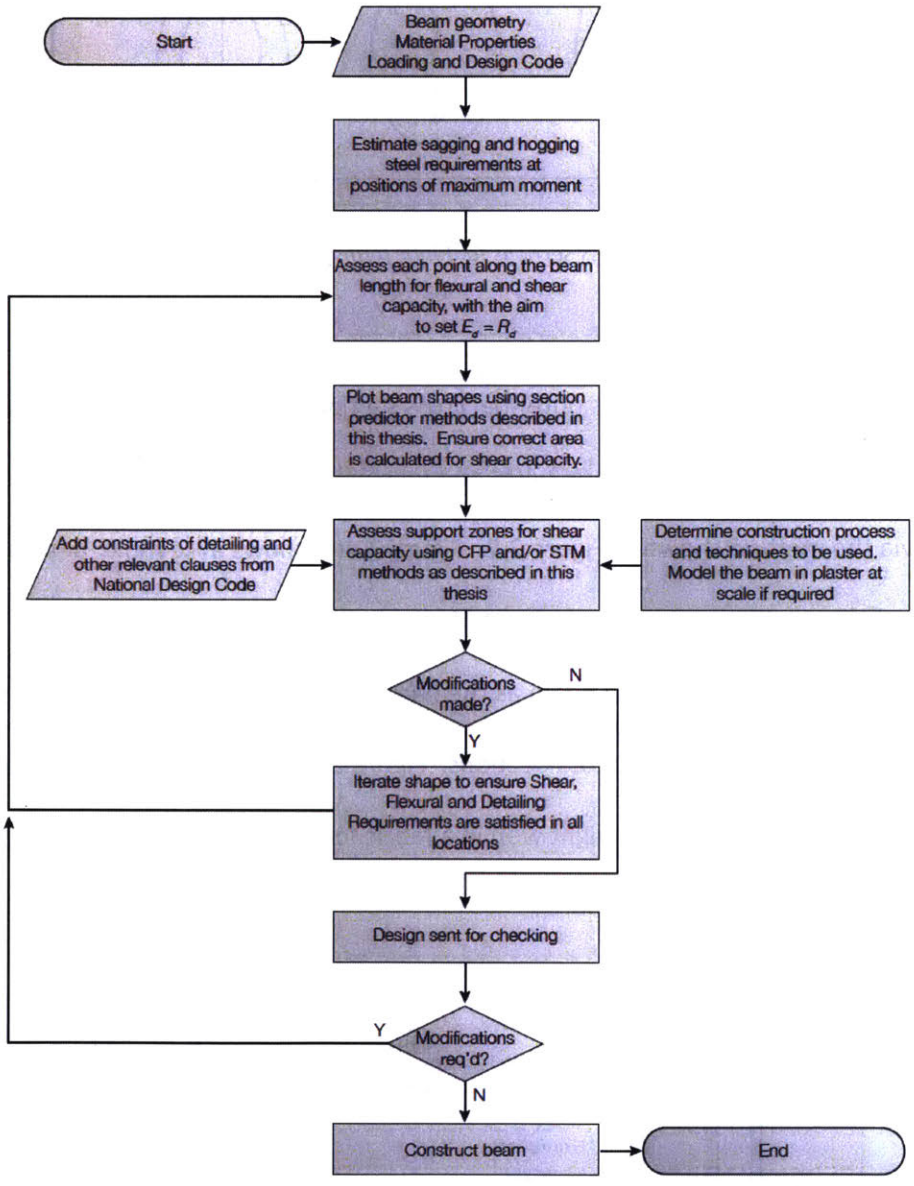

Figure 2.6: Design Flowchart for Fabric Formed Beams (Orr, 2012)

The design process is generally applicable to various beam types. It follows a sectional approach, designing each portion of the beam for the flexural and shear stresses that portion experiences. Figure 2.7 shows a diagram of the stress-strain model that is used to create the profile and predict the behavior and loading within the beam. While this is focused on a fish belly beam, the principle can still be applied to other cross-sections.

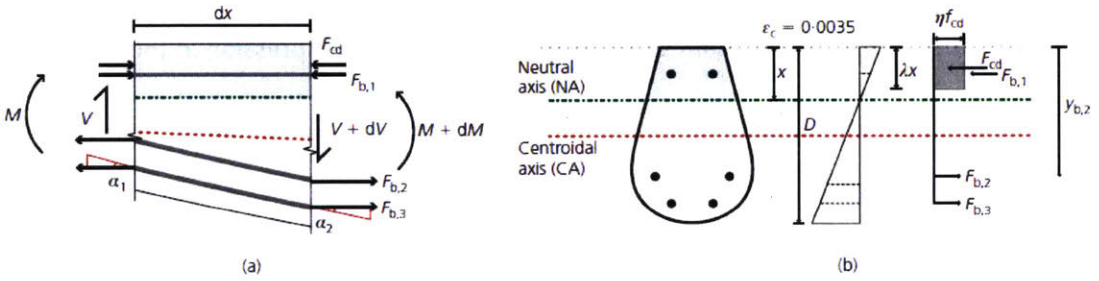

Figure 2.7: Diagram of 'fish belly' beam with passive tensile and compressive reinforcement, from Orr et al. (2014)

Via these optimized shapes and methods, (Orr, 2012) demonstrated that material savings of up to 40% are possible thus significantly reducing material costs, building weight, and the total embodied carbon of the building environment.

However, in every paper so far found, all the reinforcement is assumed to be passive. There has yet to be a study of the combination of fabric forms with actively prestressed reinforcement. Orr (2012) expresses that one logical expansion of this work would be to explore the realm of prestressing. This thesis is an initial step into that.

2.2 Prestressing

Eugene Freyssinet is often considered the founder of modern prestressing, placing the first patents on the technology. With this knowledge, he was able to overcome the perceived

limits of concrete to make record-breaking spans again and again in the mid-20th century (Shushkewich, 2012).

Concrete's strength in compression is countered by it weakness in tension. Usually this is resolved by placing steel reinforcement in the tension zone of a beam, assuming the section cracks below the neutral axis and that the reinforcement takes all of the tension.

However, in prestressing, the reinforcement has an initial tension in it, and once released, it compresses the beam so that there is additional compression in the concrete. If executed carefully, a beam could have no net tension in its section, and thus no cracking. This technology has been proven to increase the spans and load capacities possible with concrete beams (Nawy, 2000).

Figure 2.8 shows the stress profile of a beam under loading and prestress. An eccentric axial load, provided by the active reinforcement, cause a net axial compression and bending moment within the beam. The bending moment, depending on the magnitude of force and the distance from the centroid of the section, can be made to effectively neutralize the bending moment from dead and live loads.

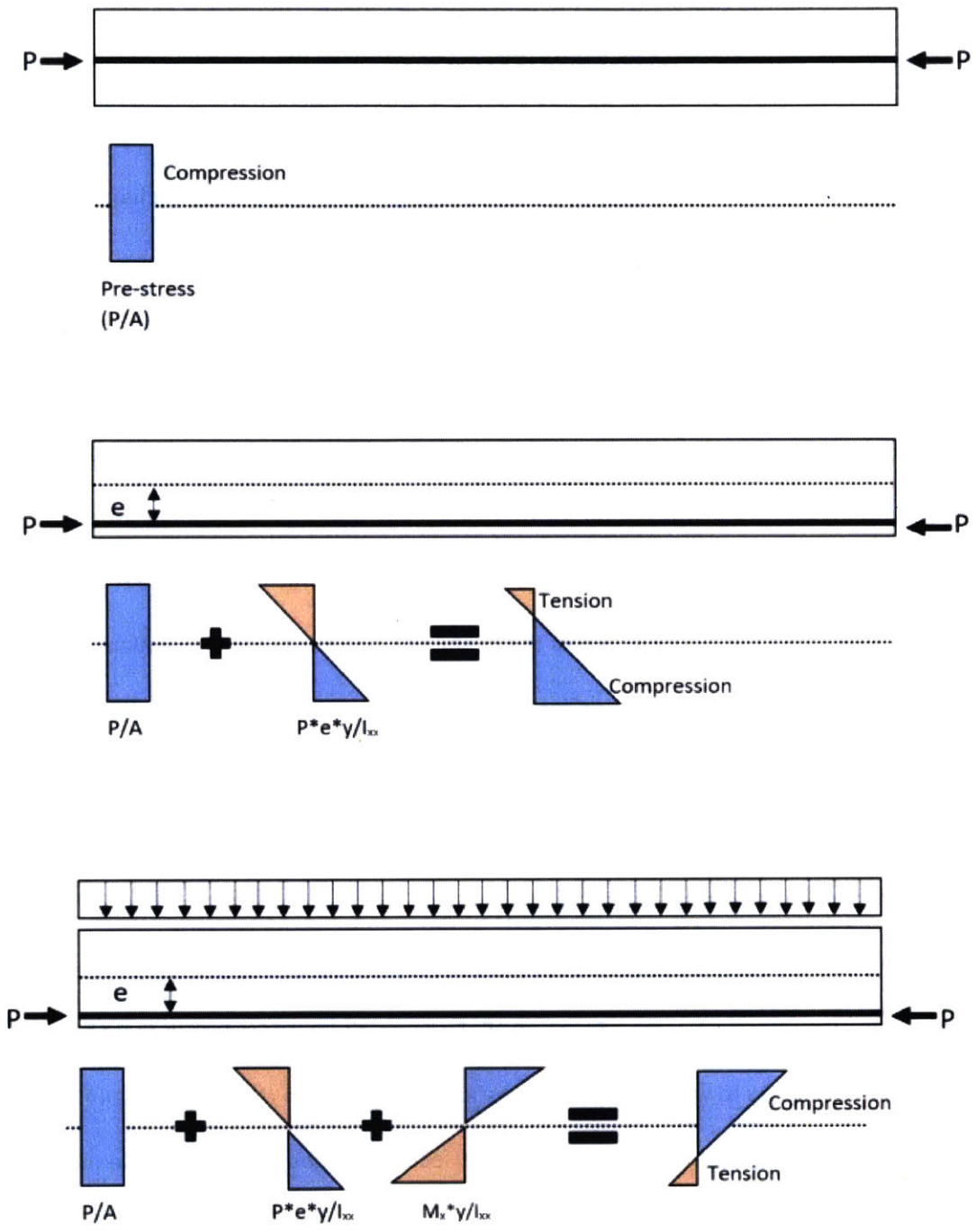

Figure 2.8: Plane-Stress diagram of prestressing a concrete beam with straight tendons, applying a compressive force P. Adapted from Hurst (1998).

There are two ways of achieving prestressing: pre-tensioning and post-tensioning. Pre-tensioning involves pulling the reinforcement taut across an anchored bed, and then pouring the

wet concrete over the cables. Once the concrete is set, the anchors are let go and the tension in the cables is transferred as compression in the section.

The second method, post-tensioning, is achieved by adding the reinforcement and prestress once the beam has been set. The beam is first cast with a duct or channel inside it, which can be made from a plastic like polyethylene/polypropylene (PPEX3) or a corrugated metal duct (Dywidag-Systems International, 2017). Once hardened, the reinforcement is threaded into the channel, and then the prestress force is applied. In pre-tensioning, the cable is held in place by its bond to the concrete along the length of the bond. In post-tensioning, anchors are placed at the ends of the beam to keep the tendon from slipping (Hurst, 1998). Grouting the channel is also an option, usually done on site, which can ensure that the prestress is transferred along the whole length of the beam, and not just at the ends (Wang et al., 2007).

One important consideration for designing with prestress is the time dependent behavior of materials and forces. Concrete usually does not reach its full strength until 28 days after casting. So prestressing too much and too early can crack or destroy the beam through hogging before it is ever fully loaded. However the prestressing force also changes over time, decreasing due to several factors. In the short term, elastic shortening, draw in of the anchors, and friction along the duct occur. These normally cause about a 10% loss in force from what is measured in the jacks to what is initially transferred to the beam (Nawy, 2000). In the long term, creep, shrinkage, and steel relaxation all effect the tendon force and cause progressive loss of prestress over its service life.

2.3 Summary

This literature review has gone over the principles of fabric formed concrete and current research. While it is expansive and comprehensive, it is limited to passively reinforced concrete.

Orr (2012) expressed that prestressed fabric formed design would be a natural extension of his work. As well, traditional prestressed design assumes that the concrete section is constant throughout. Catalogues in the PCI handbook (1999) and Nawy (2000) all show beams that are essentially extrusions of a section. The tendon may change its eccentricity along the span, but the concrete element is otherwise uniform. This thesis then will look to merge the variable sections of fabric forms with active reinforcement.

For the purposes of this paper, post-tensioning will be the chosen method of applying prestress to the tendons. In pre-tensioning, vertical hold-downs must be in place to achieve the appropriate curvature of the tendon. To achieve the variable tendon eccentricity proposed in the following sections, pre-tensioning would require an excessive amount of hold-downs, which may also need to penetrate the fabric acting as the form. With post-tensioning, the integrity of the fabric form and the changing tendon eccentricity can be achieved without impeding the construction of the beam.

3. Methodology

This chapter will go over the calculation methods used to design and analyze the various beams. The beams will be designed based on the sectional process outlined in Orr et al. (2014). The midspan is assumed to be the critical section, as tends to be true for variable-eccentricity prestressed beams (Nawy, 2000). Once the midspan is designed, the remainder of the beam sections are designed in a similar way to the midspan. Deflections are calculated in two ways to check for serviceability. Finally, one set of beams will be compared against two traditional designs, a rectangular beam and an I-beam, to assess their efficiency and performance. The traditional designs have a constant cross-section along the span, unlike the fabric formed beams.

The beams are assumed to be simply supported, uniformly loaded, and only designed for flexure. Also, to ensure cohesion of the tendon in the post-tensioning duct, it is assumed to be grouted once constructed.

3.1 Variables

In analyzing the beams, several variables were explored. All beams had varying spans between 20 ft to 50 ft (6.1m -15.2 m). The first set of beams use 5000 psi (34.5 MPa) concrete and have a varied load due to the size of the tributary area. The bay length-to-width ratio varies between ½, ⅓, and ¼.

Second, beams with varying concrete strengths are designed, all with a bay length-to-width ratio of ⅓. One set has their span-to-depth ratio constrained to 20, as though as though architectural constraints required a certain depth. The other set has a varying span-to-depth ratio, to be as materially efficient as possible.

3.2 Loads and Load Cases

The dead loads include the self-weight of the beam, as well as 3 inches of concrete deck topping to support the floor, with an assumed normal-weight concrete density of 150 pcf (2,403 kg/m^3), which results in an additional 37.5 psf (1.8 kN/m^2) of dead load on the beam. A live load of 80 psf (3.83 kN/m^2) was imposed, equal to the IBC loading for a corridor (International Code Council, 2012). Because of the precise nature of prestress calculations, there are no factors to adjust the loads for safety. Rather, minimum and maximum stress profiles are used to design the beam. This will be the maximum hogging moment and sagging moment, accounting for the most extreme stress profiles.

There are three load cases to test for each beam. The first is when the post-tensioning force is first transferred to the beam, and the maximum hogging stress is present. The prestress is at its highest and the concrete at its weakest. The second stage is when the beam is in transport from the prestressing yard to the construction site. In this case, the steel has relaxed some and the concrete has gained strength, but has no service loads on it and may still be susceptible to hogging. The third and last stage is when the beam is in service. The maximum sagging load is applied, with both dead and live load present.

3.3 Concrete Properties

The concrete properties are determined via the strength of an assumed cylinder. Below are the equations for compressive and tensile strengths of concrete given the compressive strength of a test cylinder (PCI Industry Handbook committee, 1999).

At Transfer:

$f'_{ci} = .75 * f'_c$ Compressive strength *Equation 3.1*

$f_{ci} = .6 * f'_{ci}$ Allowable compressive stress *Equation 3.2*

$f_{ti} = 6 * \sqrt{f'_{ci}}$ Allowable tensile stress *Equation 3.3*

After 28 days (curing):

$f'_{ci} = .75 * f'_c$ Allowable compressive stress *Equation 3.4*

$f_{ci} = .6 * f'_{ci}$ Allowable tensile stress *Equation 3.5*

The stresses in the extreme fibers of each beam will be checked against the allowable stresses as calculated with the above equations. For example, in the transfer stage, the top fiber is checked for tension failure, the bottom fiber for compressive failure as would happen in a hogging moment.

3.4 Beam Shape

The beam was chosen to have a 'keyhole' shape, as seen in Figure 3.1 and Figure 3.2 which is modeled after the shape from Garbett et al. (2010) in Figure 2.4(e). This shape was chosen as the most ideal because it had a high moment of inertia for a given amount of material, being so close to an I-beam. As well, the shape of the bottom chord would ideally encase a duct for a post-tensioning tendon.

Along the span, the profile of the beam is made to be parabolic with a uniform top flange. The bottom chord and top flange are assumed to be constant throughout the section. To achieve the parabolic shape, the web height is changed appropriately to ensure the bottom fiber follows a parabolic path, and that the web height is zero at the supports. The beam will be modeled in a discretized fashion, discussed more in section 3.6. The prestressing tendon is

assumed to follow a profile similar to the bottom of the beam. This makes the beam a 'variable eccentricity beam.'

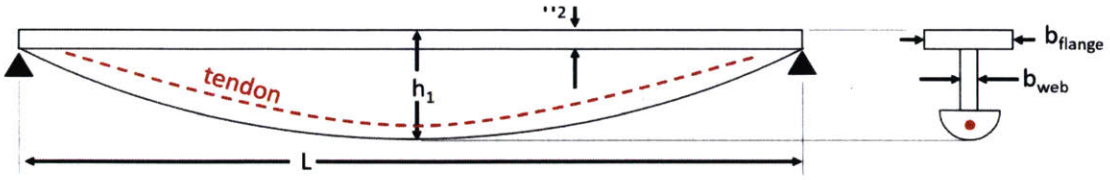

Figure 3.1: Elevation and Section view of keyhole beam

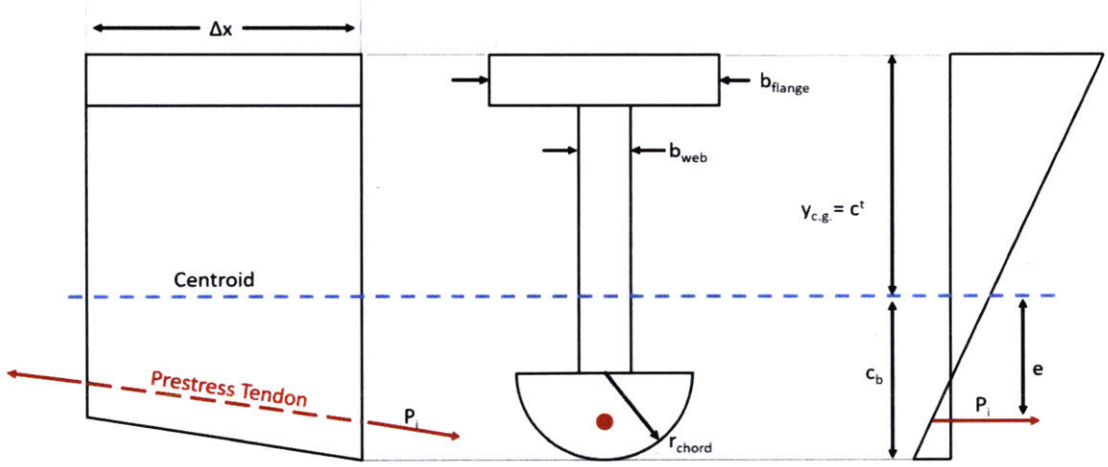

Figure 3.2: Cross Section with Prestressing tendon highlighted.

For simplicity, the bottom chord of the beam is assume to take a parabolic shape, mimicking the moment diagram due to uniform loading. While there are more intricate forms of optimizing the depth along the span, this is meant to be a first approximation to assess thefeasibility of this technology. Equation 3.6 shows the formula for the parabolic curve using the dimensioned parameter of the beam seen in Figure 3.1.

$$y(x) = \frac{h_1 - h_2}{(L/2)^2} * \left(x - \frac{L}{2}\right)^2 + h_2$$ *Equation 3.6*

To have a consistent sizing and to reduce variability between sections, the web thickness (b_{web}) and flange thickness (h_2) are both set as 25% the flange width (b_{flange}). The web thickness is checked for shear strength and increased if necessary as shown in section 3.6.

3.5 Stress Calculations

The analysis of each beam was done in an Excel spreadsheet. This ensures that the barrier of entry for future engineers or researchers is reduced. Another motivation was to make sure that the calculations were well understood and that the analysis could be reproduced without the need for specialized software.

First a span is chosen and the appropriate forces are calculated: the service dead load moment from the slab and the live load moment. The anticipated weight of the final beam is estimated, and from this the self-weight moment is calculated. The critical section is assumed to be the mid-span to start the calculations.

Now knowing the specific loading for the given span, the minimum required section moduli are calculated via Equation 3.7 and Equation 3.8 below. Gamma (γ) is the remaining fraction of prestress force after initial losses. It is assumed that γ = 82% based on examples in Nawy (2000).

$$S^t\ minimum = \frac{(1-\gamma) * M_{Self\ Weight} + M_{Service\ Dead} + M_{Live}}{\gamma f_{ti} - f_c}$$ *Equation 3.7*

$$S_b\ minimum = \frac{(1-\gamma) * M_{Self\ Weight} + M_{Service\ Dead} + M_{Live}}{f_t - \gamma f_{ci}}$$ *Equation 3.8*

These values are used as an initial benchmark to check the section of the beam. The geometric properties of the beam must at least meet these criteria to be safely used. Once

these values and the loadings are calculated, a beam section is chosen based on three variables: B_{flange}, h_1, and r_{chord}. From these values, the appropriate geometric properties are calculated automatically.

With a trial shape established, the assumed weight is changed to match the calculated weight, and the required minimum section moduli are updated. The depth and sizing of the beam are iterated until this first check is satisfied.

Next, the prestressing force and eccentricity are determined. Since prestressing requires prefabrication, there exist many standardized beams. Some organizations like the Prestressed Concrete Institute (PCI) provide design charts and tables to facilitate the design for specific loadings once a section is chosen. However in this case, the eccentricity and prestress force must be checked with analysis.

An eccentricity and prestressing force are chosen. The excel document calculates the stresses of the extreme fibers in the three critical loading stages according to the following formula, where compression is negative:

At Transfer:

$$f^{top} = \frac{-P_i}{A_c} + \left(\frac{P_i * e * c_t}{I_{xx}}\right) + \frac{-M_{SelfWeight}}{S^{top}} \qquad \textit{Equation 3.9}$$

$$f_{bottom} = \frac{-P_i}{A_c} + \left(\frac{-P_i * e * c_b}{I_{xx}}\right) + \frac{M_{SelfWeight}}{S_{bottom}} \qquad \textit{Equation 3.10}$$

During Transport:

$$f^{top} = \frac{-P_e}{A_c} + \left(\frac{P_e * e * c_t}{I_{xx}}\right) + \frac{-M_{SelfWeight}}{S^{top}} \qquad \textit{Equation 3.11}$$

$$f_{bottom} = \frac{-P_e}{A_c} + \left(\frac{-P_e * e * c_b}{I_{xx}}\right) + \frac{M_{SelfWeight}}{S_{bottom}} \qquad \textit{Equation 3.12}$$

While in Service:

$$f^{top} = \frac{-P_e}{A_c} + \left(\frac{P_e * e * c_t}{I_{xx}}\right) + \frac{-M_{total}}{S^{top}} \qquad \textit{Equation 3.13}$$

$$f_{bottom} = \frac{-P_e}{A_c} + \left(\frac{-P_e * e * c_b}{I_{xx}}\right) + \frac{M_{total}}{S_{bottom}} \qquad \textit{Equation 3.14}$$

Where:

$$P_e = \gamma * P_i \qquad \textit{Equation 3.15}$$

The first term in each equation accounts for the compressive stress due to post-tensioning. The second term accounts for the stresses of the hogging moment caused by the eccentricity of the tendon. The last term accounts for the stresses from the bending moment caused by the gravity loads on the beam.

The stresses of these extreme fibers are checked against the compressive or tensile strength of the concrete as determined in section 3.4. The force and eccentricity is iterated until a safe section for the mid-span is achieved. To make sure the section is constructible, the required tendon area is calculated. The tendon steel is assumed to have a tensile strength of 270,000 psi (1861 MPa), with a maximum allowable tensile stress of 189,000 psi (1303 MPa), or 70% of the strength (Nawy, 2000). The minimum area of steel is calculated, and then checked to make sure that the minimum amount of cover is achieved. According to ACI 318-14, the minimum cover for a prestressed concrete beam not exposed to weather is the larger of 5/8" (16 mm) or the diameter of the tendon used (American Concrete Institute, 2014).

3.6 Sectional Design

With the mid-span section properties determined, the next step is to create the rest of the beam. Using the principle of iterative, sectional design by Garbett et al. (2010) and Orr (2012), the beam is split into 24 sections, and each of these pieces is individually analyzed. The depth of the section is automatically calculated using Equation 3.6 and its loading is determined by its distance from the support. Only 12 sections are analyzed on each side, since the beam is symmetrical.

With this done, the eccentricity of the tendon is chosen. The prestress force is constant throughout the length of the beam. While in actuality, the prestress force is at an increasing angle the closer it comes to the supports, the prestress force at each piece is approximated as horizontal to simplify calculations. While choosing different eccentricities, the stresses of the extreme fibers under the three loading conditions are calculated as the mid-span section was. This is done until all sections satisfy the stresses do not exceed the limitations set by section 3.3.

Lastly, shear strength of the web is calculated to ensure that it has appropriate thickness. Equation 3.16, from Nawy (2000), is used to calculate the shear capacity of the web and takes into account the upwards force of the harped tendon. The web thickness is increased until the shear strength is met. This will primarily affect the web near the supports, where shear stress is highest.

$$V_c = \left(3.5 * \sqrt{f'_c} + .3 * \overline{f_c}\right) * (b_{web} * .8 * h) + V_p \qquad \textit{Equation 3.16}$$

3.7 Deflection Calculation

While strength is a crucial detail in determining the feasibility of a beam, its serviceability is also a large aspect. Often times, deflection is the controlling factor in a beam or column design. As such, the deflection of each beam is calculated in two ways. Then it is compared to the deflection limit set by IBC: $\Delta_{MAX} \leq L/360$. The Young's Modulus (E_c) of concrete is calculated by Equation 3.17, where the density is in pcf and f'_c is in psi. Deflection of a simply supported beam under uniform loading is calculated by Equation 3.18.

$$E_c = (33 * {w_{conc}}^{1.5}) * \sqrt{f'_c} \qquad \textit{Equation 3.17}$$

$$\Delta_{max} = \frac{5}{384} * \frac{q_L * L^4}{E_c * I_{xx}} \qquad \textit{Equation 3.18}$$

Since each section has already had its moment of inertia calculated, a quick approximation for the deflection is to average the moment of inertia for each section, and then input the average I value Equation 3.18. This is a conservative approximation for two reasons. The first is that it does not account for the upwards camber from the prestressing tendon. The other reason is because it approximates the beam as one with a uniform section, as shown in Figure 3.3. Where the moment is highest, there is actually more depth, and thus rigidity to the beam, and vice versa for the ends of the beam. Thus the actual rigidity is significantly under-estimated by this method.

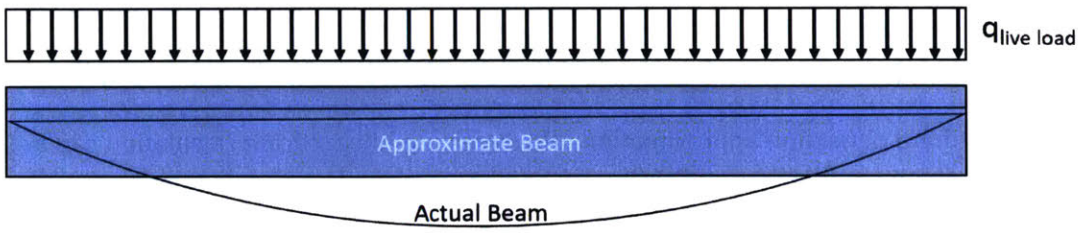

Figure 3.3: Overlay of approximate beam calculated by Equation 3.18 and the designed beam

The second method of deflection calculation is through energy methods. The energy of the work done by loading must be equal to the potential stored energy of the beam deflection.

$$\int_0^L q * u(x)dx = \int_0^L \frac{M_x(x)^2}{2 * E_c * I_{xx}(x)}\, dx \qquad \textit{Equation 3.19}$$

Since the beam is already discretized, the integral can be written as a sum using the properties of each section that have already been calculated. Below is the progression from the initial summation to the downward deformation of a given beam segment, *n*.

$$\sum_{i=1}^{n} q * u_i * \Delta x = \sum_{i=1}^{n} \frac{{M_{x,i}}^2}{2 * E_c * I_{xx,i}} * \Delta x \qquad \textit{Equation 3.20}$$

$$\sum_{i=1}^{n} u_i = \frac{1}{2 * E * q} * \sum_{i=1}^{n} \frac{{M_{x,i}}^2}{I_{xx,i}} \qquad \textit{Equation 3.21}$$

$$u_n = \frac{1}{2 * E * q} * \sum_{i=1}^{n} \frac{{M_{x,i}}^2}{I_{xx,i}} - \sum_{i=1}^{n-1} u_i \qquad \textit{Equation 3.22}$$

For each section the cumulative deflection is calculated, until the mid-span deflection is reached, and this is the value compared against the IBC limit. This calculation is also conservative because it discounts the hogging camber from prestressing. However it is more

accurate than the rectangular beam approximation due to the fact that each section is matched with its appropriate loading. It is believed that the 12 sections the half-span is split into is sufficient for a deflection approximation. However, a more accurate calculation can be made with a higher resolution of discretization.

3.8 Efficiency Measure

To measure the potential efficiency of this merging of technologies, the weight and prestressing force for beams of more conventional designs should be compared. One set of beams, the 5000 psi (34.5 MPa) strength with a ⅓ bay-width ratio, will be designed with two different sections, which will be uniform across the span, as in Figure 3.4. One will be a rectangular beam, and the second will be a symmetric I-beam, where the flange and web thickness will also be 25% of the b_{flange} for consistent proportions with the fabric formed design. To ensure appropriate comparisons, the midspan depth (h_1) of each of the conventional designs will be the same. All other dimensions will be adjusted to reduce weight and prestress force in each respective design. The I-beam will likely have a higher moment of inertia than the fabric formed beam of the same depth. However, the material saved in the cross section for the I-beam may be different than the material saved across the span for the fabric formed beam. This trade-off is of primary interest.

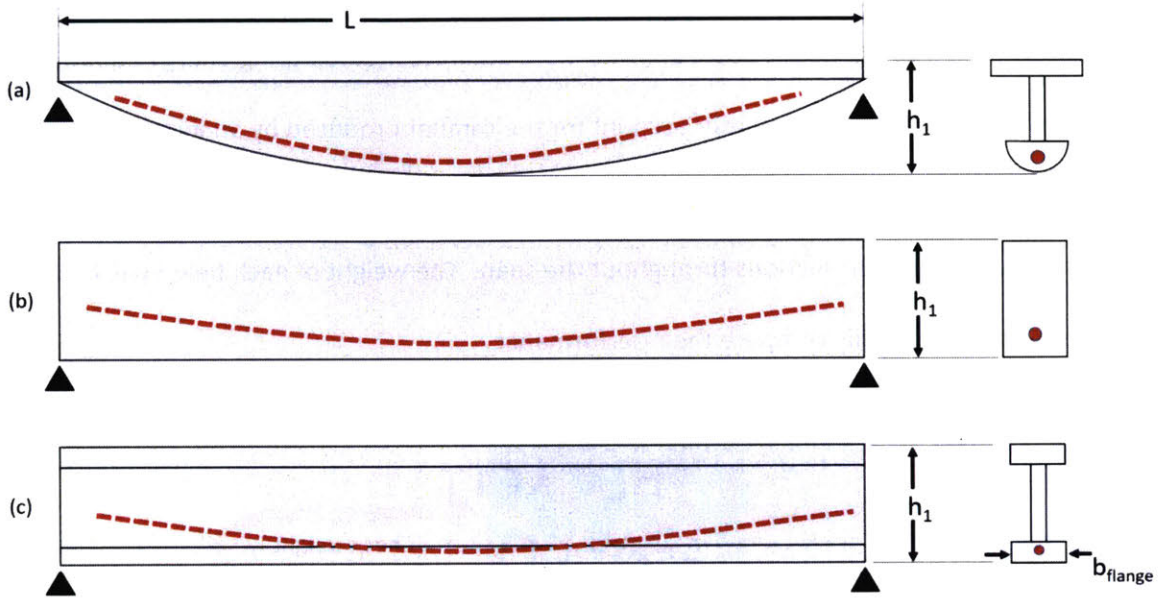

Figure 3.4: comparison between (a) fabric-formed beam, (b) rectangular beam, and (c) I-beam

3.9 Summary

The various beams will be designed by a sectional process. The span is first split into 24 sections, but only half the span is designed under the assumption of symmetry. The midspan, assumed to be the critical section, is determined first, by calculating the largest stresses under loadings that cause maximum hogging and sagging deformations. This section is iterated, attempting to minimize both the section weight and prestress force required. Once an appropriate midspan section is designed, the rest of the beam is determined via a similar method. The depth is predetermined by the parabolic equation of the bottom fiber, while the tendon eccentricity and web thickness are chosen to satisfy stress criteria. The beams are designed under various constraints and variables, including different bay sizes, concrete strengths, limiting span-to-depth ratio, constraining prestressing force, etc. Figure 3.5 summarizes this procedure.

The deflection of the beam is calculated in two ways, one using a simplified approximation of the beam, and a second, more accurate method using energy equations. Both are conservative, because neither account for the camber produced by an initial prestressing of the tendon. To check the efficiency, one set of beams will be compared against more traditional designs with constant sections throughout the span. The weight of each beam will be divided by its span to more easily compare their performance.

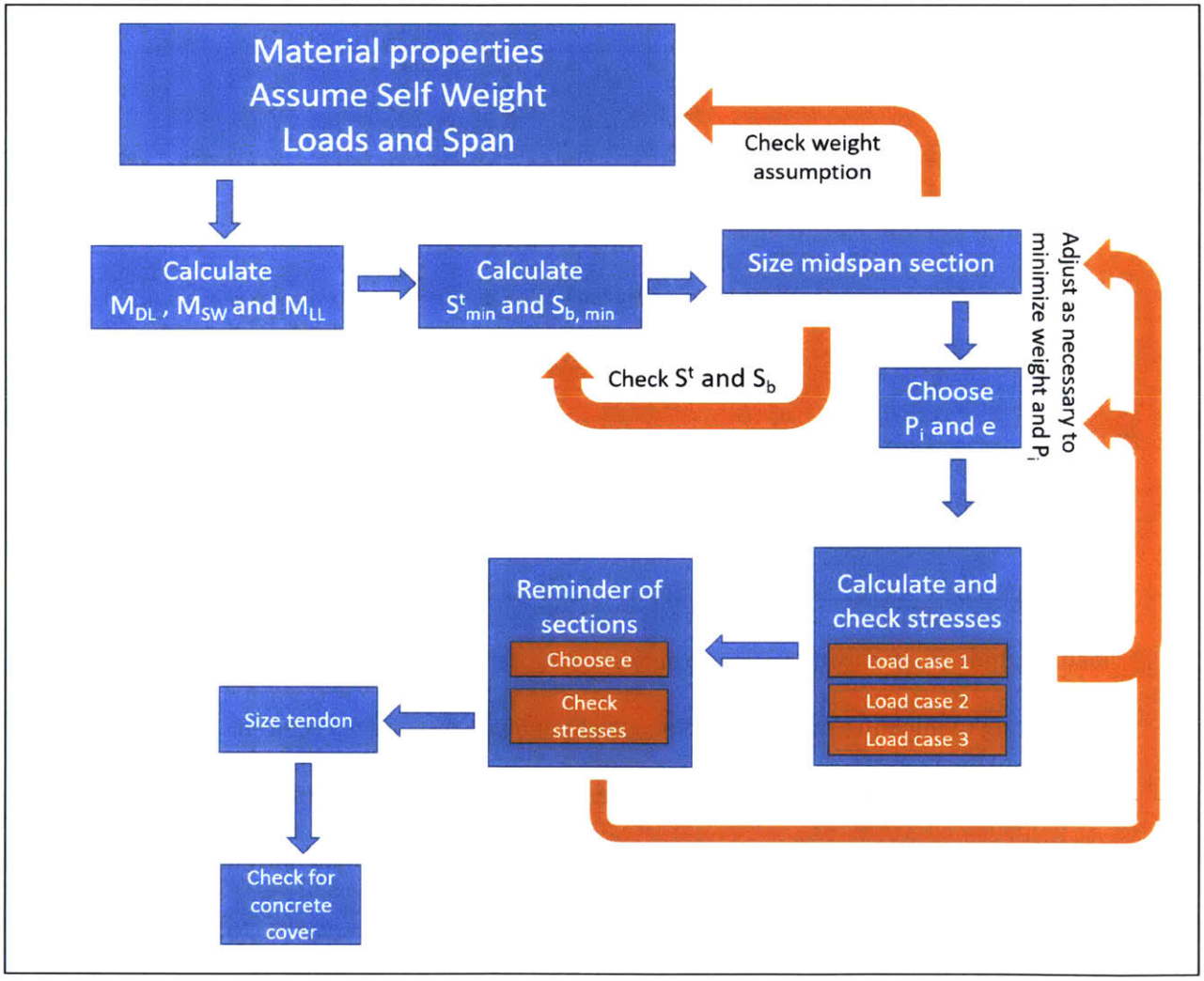

Figure 3.5: Flow chart for prestressed beam design.

4. Results

This chapter will show the beam designs and their various properties and performances. First beams of the same strength are subject to different loadings via a changing bay size. Next, beams of varying concrete strength under a fixed bay size are examined. The first set of these is constrained to have a span-to-depth ratio of 20, as though architectural constraints require this. The second set of beams with varying strength are allowed to have varying depths, but the prestressing force for each span is locked to be the same as the force determined in the lowest concrete strength beam. Lastly, a set of beams are compared against more traditional designs to assess their potential efficiency.

In Appendix A, numeric tables are included which document the final results of the beam analyses. This includes dimensions, prestressing forces, deflections, spans, and strengths. There is also a walkthrough of a specific beam design in Appendix B.

4.1 Discussion

4.1.1 Varying Bay Size

The beams in this section are designed using a concrete strength of 5000 psi (34.5 MPa), and are loaded with varying bay width ratios of ½, ⅓, and ¼. Figure 4.1 and Figure 4.2 show the prestressing force and span-to-depth ratio respectively. In varying the bay size and thus the loading, the prestress force must increase in order to account for the increased stress. This is as expected and the forces required are reasonable. This is likely because the prestress force is primarily determined by the midspan section's requirements, and becomes much less relevant closer to the supports.

The span-to-depth ratio of the beams also follows a fairly predictable trend, however, to achieve the required strength in safety, the L/2 bay size must have a large depth in order to counter the higher loads, and depending on constructability requirements, this may be an infeasible beam spacing. It is possible to use a higher strength concrete, and thus a higher prestress to reduce the midspan depth. However that reduced depth may increase deflection. This relation between strength, depth and deflection is reviewed in section 4.1.2.

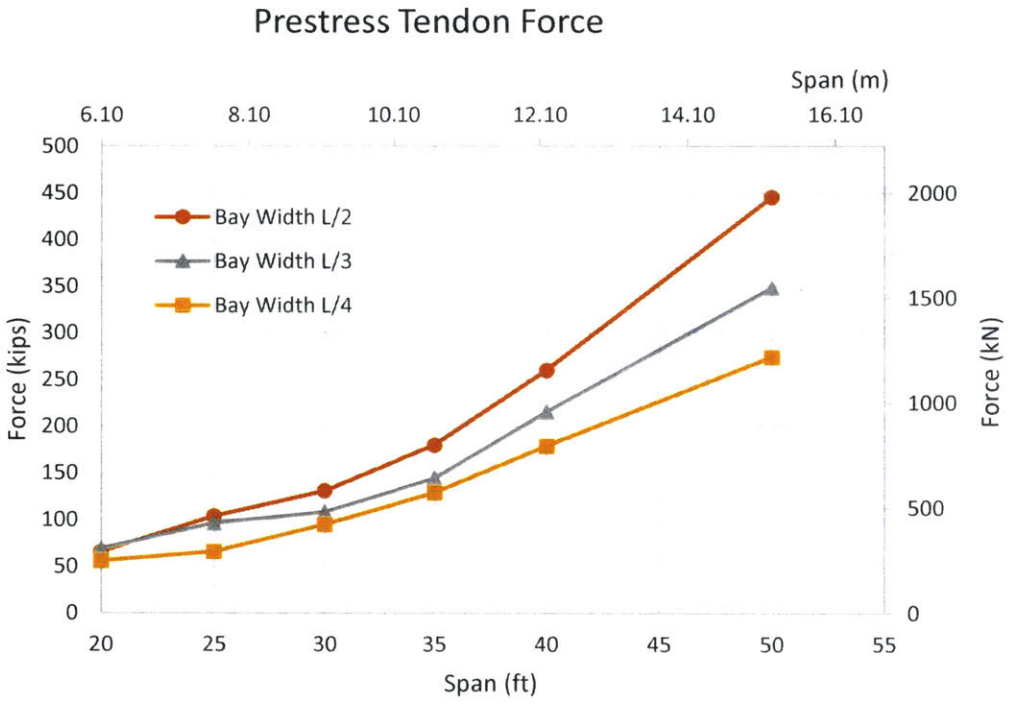

Figure 4.1: Prestressing Force versus the bay size for 5000 psi (34.5MPa) concrete

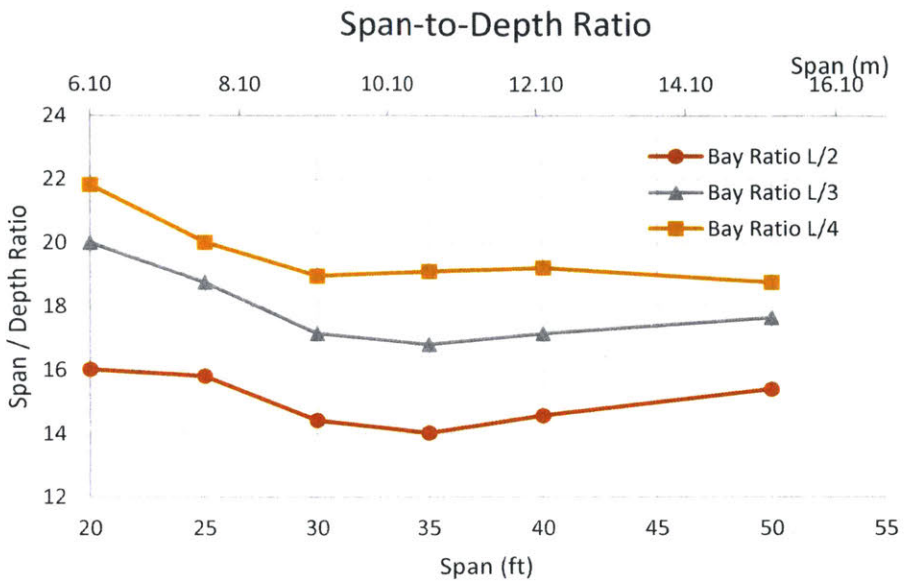

Figure 4.2: Span-to-depth ratio versus the bay size for 5000 psi (34.5 MPa) concrete

Figure 4.3 and Figure 4.4 show the live load midspan deflections plotted against the L/360 limit set by IBC (2012). Both deflection calculations show that these beams are within the limit set by IBC. The deflections calculated by Equation 3.18 show a trend that follows closely with the IBC limit. Interestingly, largest bay size and loading has the largest margin for deflection. The large span-to-depth ratio for these large bays likely lead to this. The energy method calculations from Equation 3.22 indicate that the deflections increase at a much slower rate than the IBC limit. If the trend in Figure 4.4 continues, a longer span will be unlikely to ever be governed by deflection. It can be suggested then that for a normal strength concrete, design will be governed by constructability concerns like maximum depth or prestress force, rather than deflection or strength.

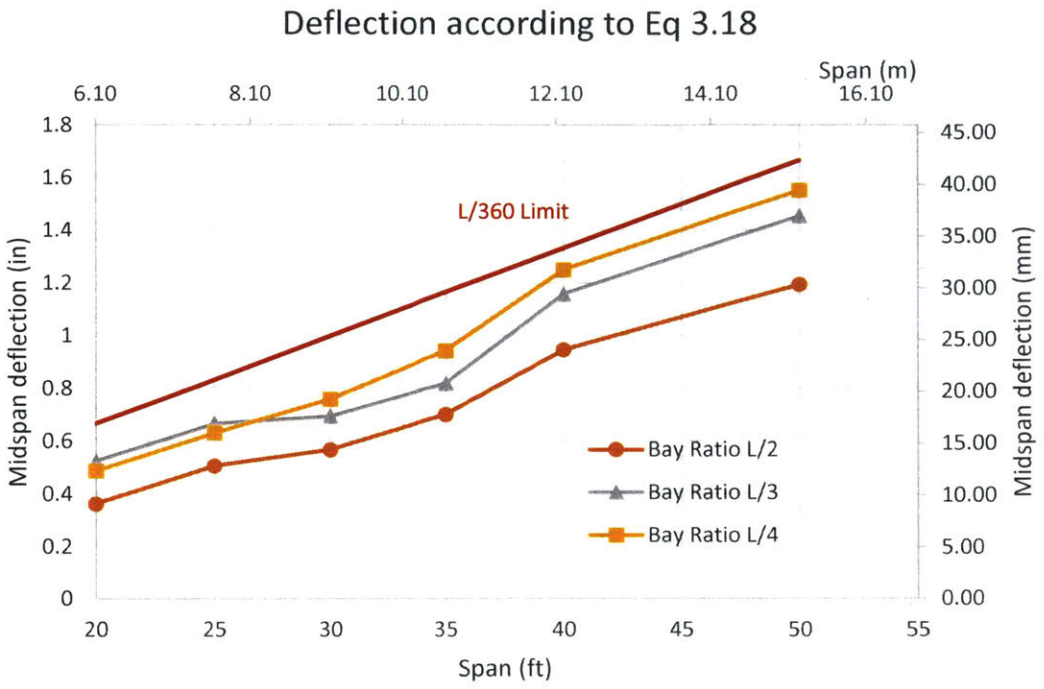

Figure 4.3: Approximate Deflection vs. the bay size for 5000 psi concrete

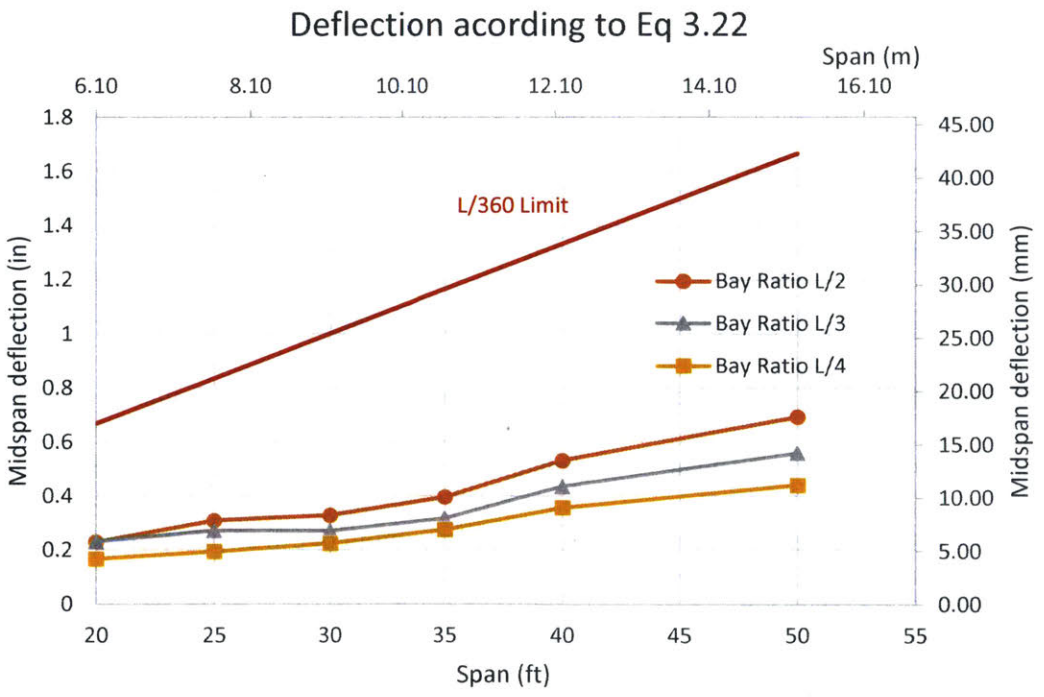

Figure 4.4: Deflection via energy methods vs. the bay size for 5000 psi concrete

Figure 4.5 shows the normalized weight of the beams. The total weight of the beam was calculated, and then divided by the total span. As expected, increasing the loading would increase the total material required. However, by doubling the spacing of beam, and thus halving the number of elements required, less than double the material is required generally. For short spans, only about 52% more material is required, and at long spans, it is 78% more material.

A designer would be recommended to choose a wider beam spacing if the maximum depth requirement were loose and the increase in prestress force was not considered critical. Also, in having fewer total beams for a structure, the erection and labor costs would decrease along with total material required.

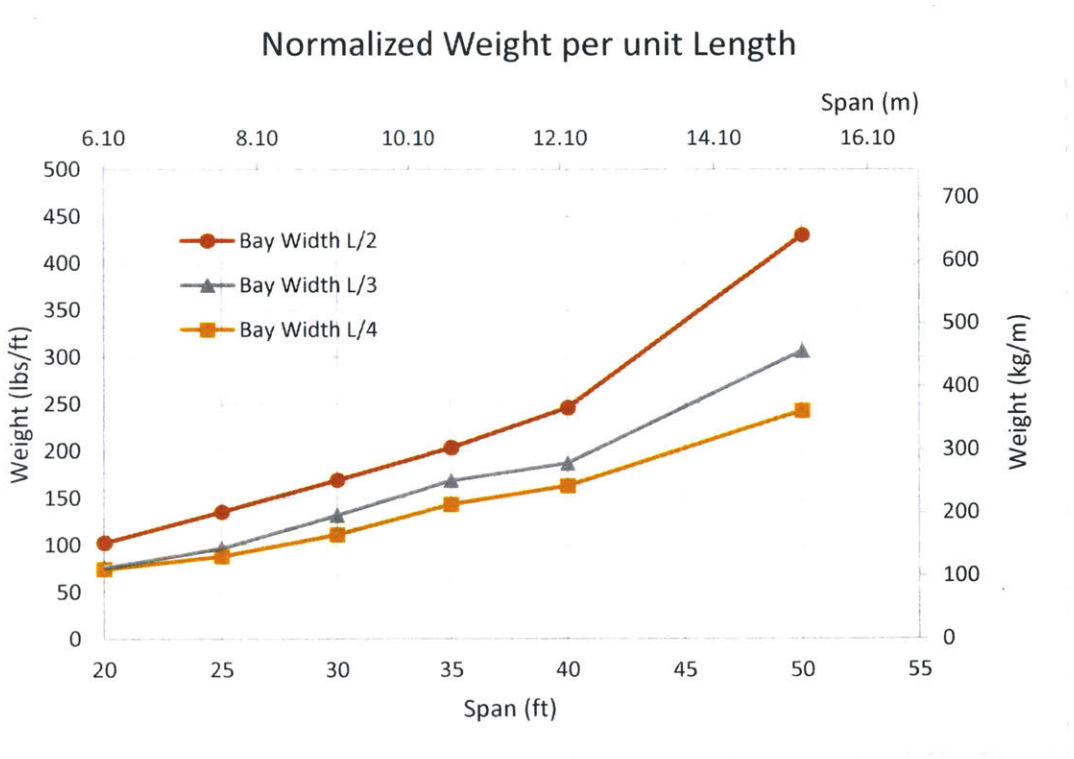

Figure 4.5: Weight per unit length versus the bay size for 5000 psi (34.5 MPa) concrete

4.1.2 Varying Concrete Strength

The following two sections cover beams that varied the strength of the concrete, between 5000 psi (34.5 MPa), 10,000 psi (69 MPa), and 15,000 psi (103 MPa) concrete. The first section constrains the span-to-depth ratio of the beams to 20. The second section releases that constraint and instead holds the prestress force for the spans constant. The bay width-to-length ratios for all following beams was set at ⅓.

4.1.2.1 Constant Span-to-Depth Ratio

Initially, the beams were constrained to have a span-to-depth ratio of 20, as though there were a constructability requirement, like ceiling height. Figure 4.6 shows the prestressing force for the various strengths. The 15,000 psi (103 MPa) concrete can use a marginally lower prestress than its weaker counterparts in the same span, but is effectively the same. The focus on minimizing beam weight caused the moment of inertia to fall, and so the same prestress would cause higher stresses in the extreme fibers. Since a stronger concrete has higher allowable stresses the net effect on prestressing force seems negligible.

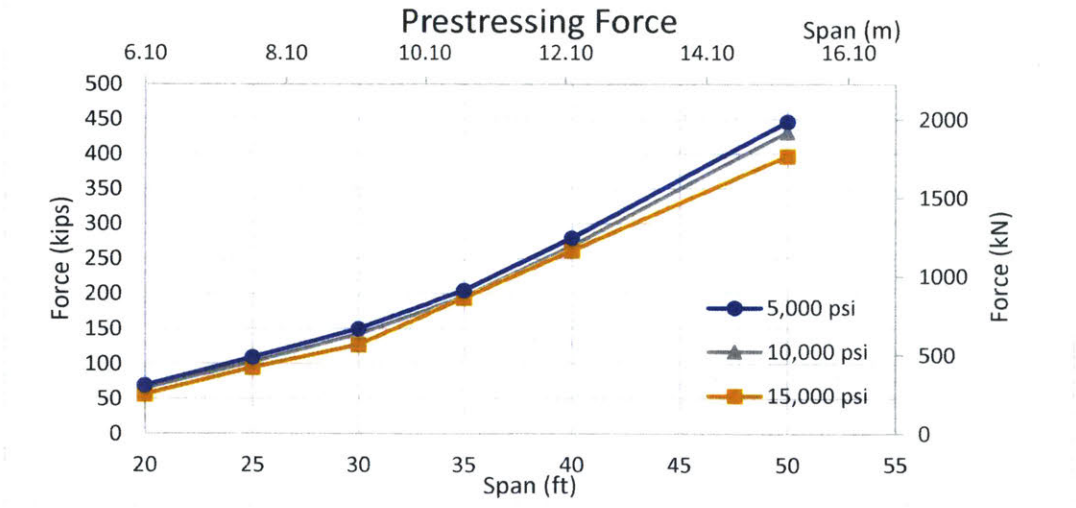

Figure 4.6: Prestressing Force for varying strengths of concrete, (span-to-depth ratio =20)

Figure 4.7 and Figure 4.8 show the deflections for these beams. Figure 4.8 is at first alarming, showing that the low-constrained depth skirts the IBC limit, with the mid strength concrete even surpassing it at higher spans. However, this being the extremely conservative calculation, it can be somewhat discounted, especially when Figure 4.8 is considered. The energy method calculations again rise at a slower rate than the limit does. Similarly to the previous section, deflection does not seem as if it would be the controlling factor, even for longer spans. In considering this and the previous section, designers can reasonably use Equation 3.18 as a first check for deflections, instead of the more laborious but accurate Equation 3.22.

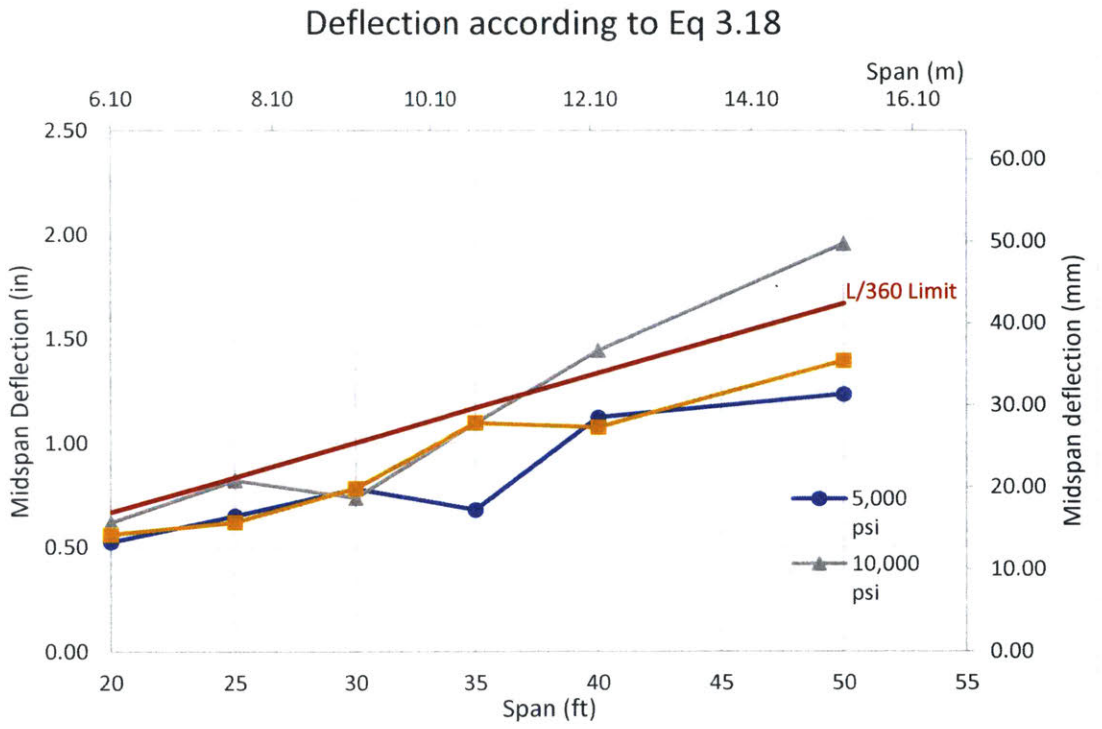

Figure 4.7: Approximate deflection for varying concrete strengths (span-to-depth ratio = 20)

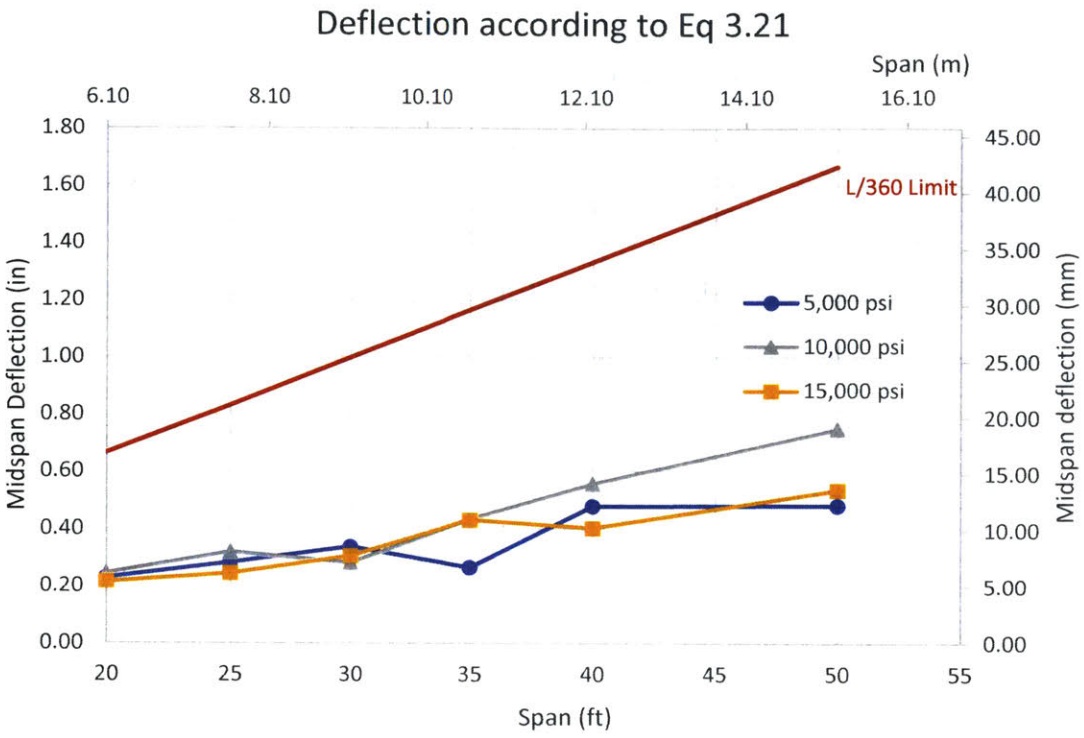

Figure 4.8: Deflection via energy methods for varying concrete strengths (span-to-depth ratio = 20)

The normalized weight of these beams, shown in Figure 4.9, display the expected trend, where stronger concrete can use less material. Somewhat surprising is the difference in weights between the strengths. There is much more saved in choosing 10,000 psi (69 MPa) concrete over 5,000 psi (34.5 MPa) concrete, around 38%. But the savings from choosing 15,000 psi (103 MPa) over the 10,000 psi (69 MPa) is much less. At a short span, it is nearly non-existent and at long spans, it is just barely 19%.

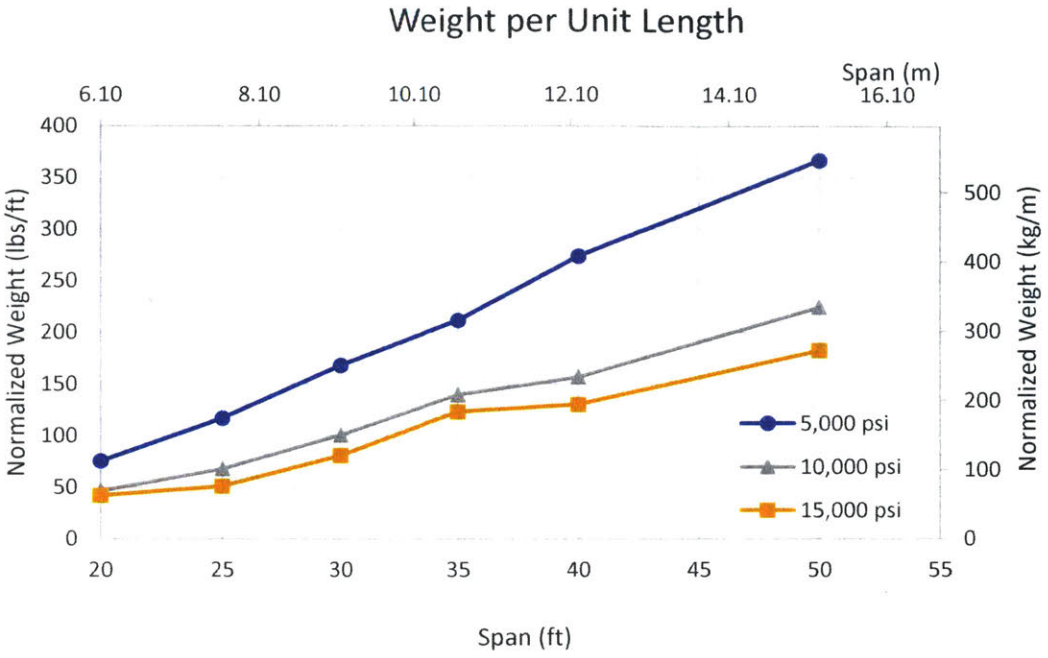

Figure 4.9: Normalized weight of beams for varying concrete strengths (span-to-depth ratio = 20)

4.1.2.2 Consistent Prestress Force

The preceding section demonstrated that prestress force essentially did not change when the depth was kept constant. So in response, another set of beams is designed with varying strengths, however this time the prestress forces are constrained, and the depths of each beam are allowed to vary. The force was set equal to the required force of the original 5000 psi (34.5 Mpa) beam for the L/3 bay size loading.

Figure 4.10 shows the span-to-depth ratios for the various strengths of concrete. When using the same prestress and allowing for variability in depth, appropriate ratios are achieved. As expected, a higher strength allows for a shallower beam. At first this suggests that the higher strengths will also have higher deflections, but this is not necessarily the case.

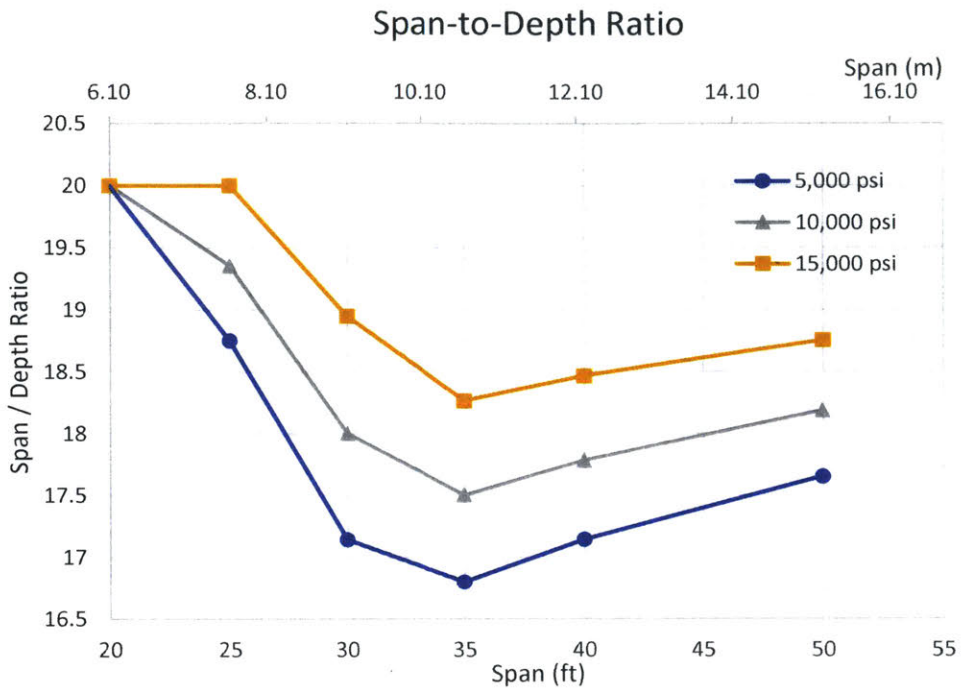

Figure 4.10: Span-to-depth ratio for varying strengths of concrete (Consistent prestress force)

Figure 4.11 and Figure 4.12 show the deflections for the constant prestress force beams. The general trend of deflection not controlling continues, with even the approximate deflection calculation below the IBC limit. Curiously though, the deflections for all the strengths is extremely similar. The reduced moment of inertia from a shallower beam seems offset by the higher elastic modulus of a higher strength concrete. Again the approximate deflections are larger than those calculated by energy methods as expected.

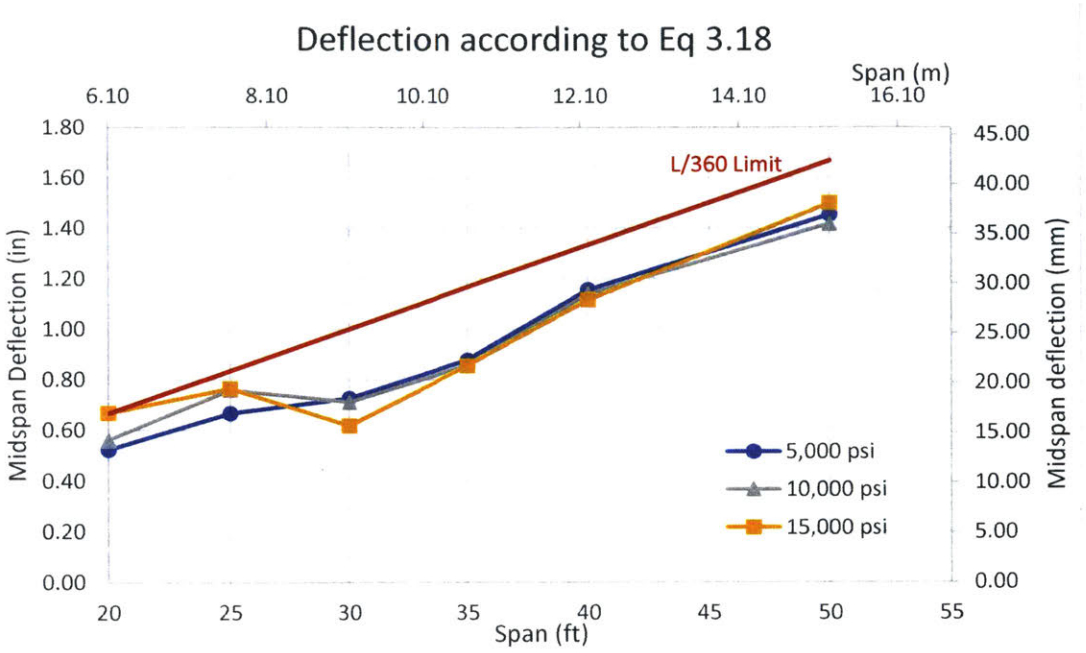

Figure 4.11: Approximate deflection for varying strengths of concrete (Consistent prestress force)

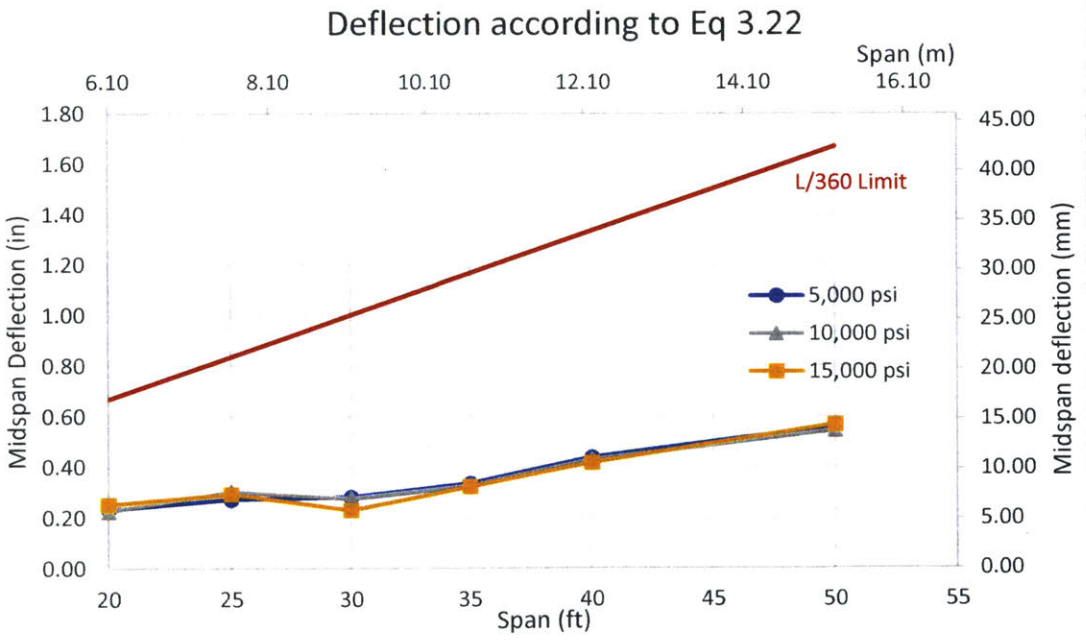

Figure 4.12: Deflection via energy methods for varying strengths of concrete (consistent prestress force)

The normalized weights of each beam follow an expected trend, as Figure 4.13 shows. The higher strength concrete allows for less material, and thus a lighter overall beam. However the savings are limited. Choosing a concrete that is three times stronger, may result in 53% less material in the shortest span, but 33% less in the longest span.

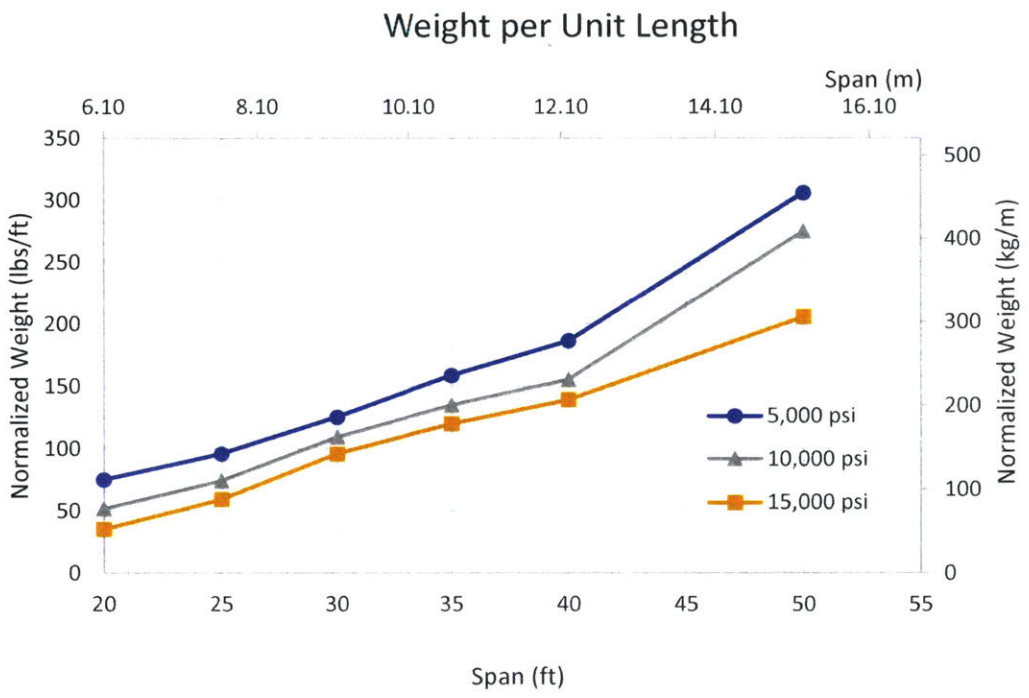

Figure 4.13: Normalized weight of beams for varying concrete strength (Consistent prestress force)

4.1.3 Beam Figures

Figure 4.14 and Figure 4.15 show some details of a chosen beam for reference. Appendix B1 includes a walkthrough calculation of this beam's design. Note that the highlighted tendon profile stays within the bottom chord of the beam section. While the figure shows a discretized form of the beam, it is apparent that the path of both the beam and tendon is very shallow and thus a continuous curve can readily be constructed from this discretization.

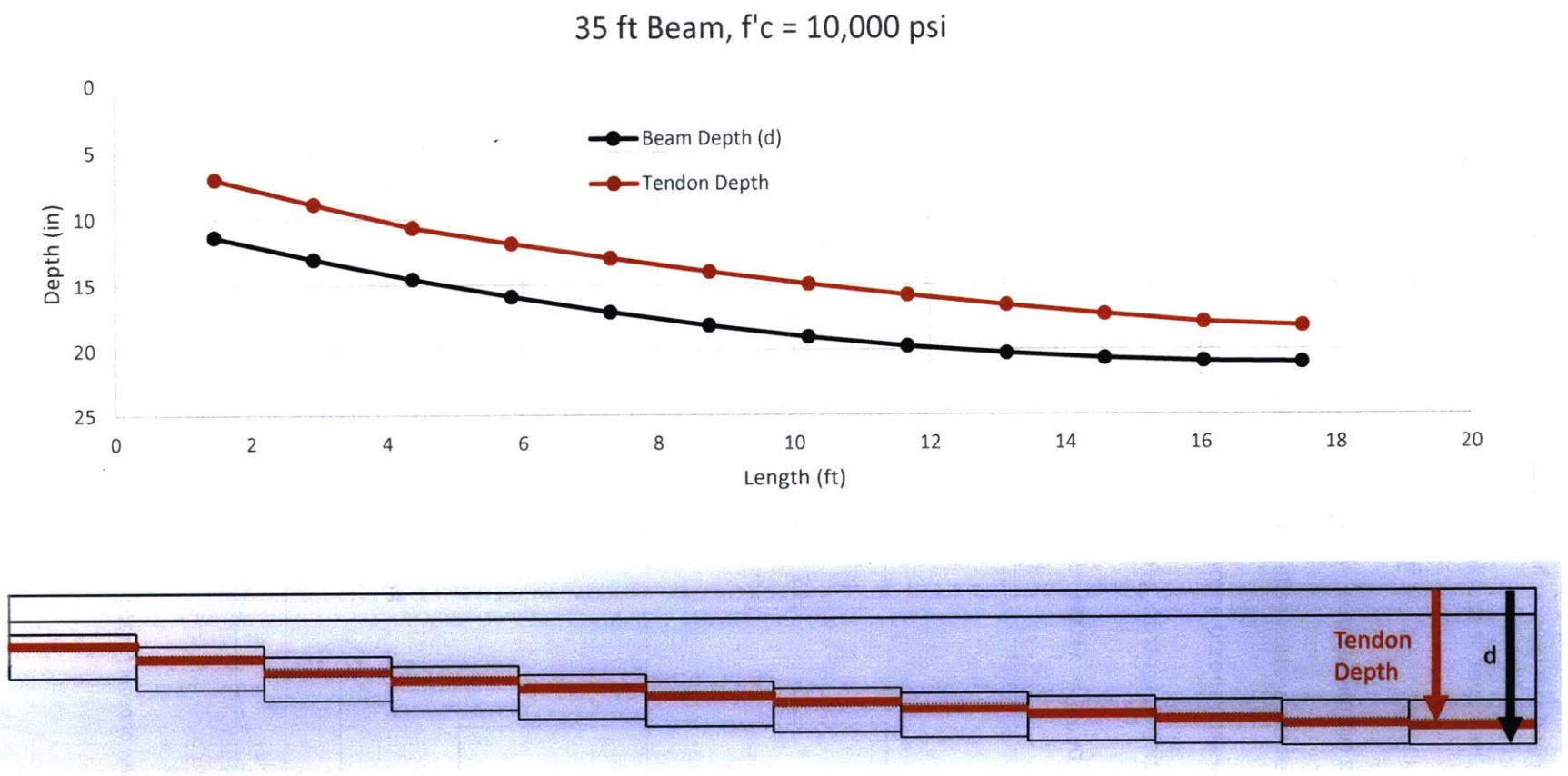

Figure 4.14: Beam profile for 10,000 psi concrete over 35 ft. (10.7 m) with span-to-depth ratio of 20

Figure 4.15 shows that the tendon has an adequate concrete cover to the bottom fiber, as outlined in ACI 318-14. However, it should be noted that the sharp corner portions of the bottom chord may be troubling to cast. At first, it was thought the bottom chord form a semi-circular shape over a more complete circle. As such the excel sheets and program calculating the geometric properties of the section reflected this. This form is still able to be constructed, but a future delve into research should account for this caveat, possibly with form-finding techniques like those developed for truss geometry in Veenendaal et.al (2011a).

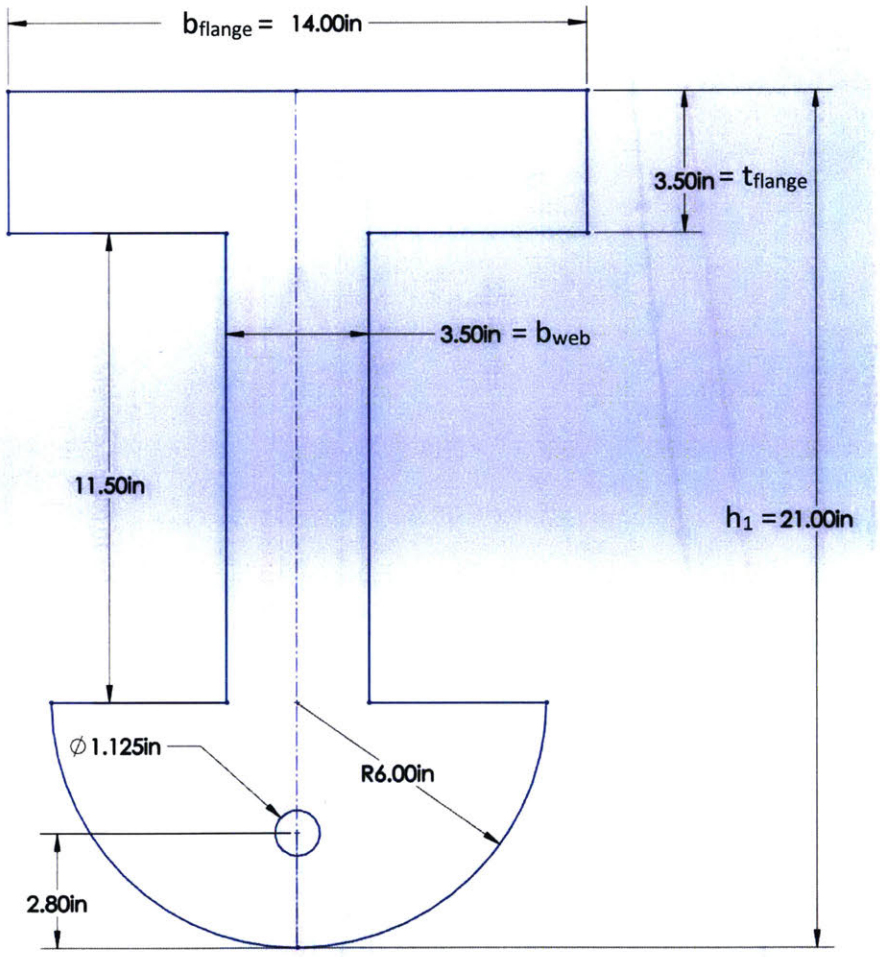

Figure 4.15: Midspan Section view of beam for 10,000 psi concrete, over 35 ft with span-to-depth ratio = 20

4.1.4 Element Efficiency

To quantify the potential material savings, two sets of more conventional, constant section beams are designed to compare against these fabric formed beams. Each beam is designed to minimize the weight used and around the critical midsection with a variable eccentricity tendon. To have a consistent comparison, they are also constrained to the same midspan depth as the appropriate fabric formed beam. Each of these are uniquely designed, instead of from a catalogue, so that weight is minimized.

Figure 4.16 shows the resulting comparison of the weight per length of span. While the fabric formed beam saves on material over the rectangular beam, it is on par with the savings of using an I-beam shape. The difference is negligible. While the fabric formed beam saves material over the length of span, the keyhole cross section is not as effective as an I-beam shape. In Figure 4.17, it can be seen that the keyhole shape is larger, mostly in the top flange and bottom chord. This added material seems to completely negate the savings across the span. Also, the material saved across the span would primarily be within the web of the section, and since the web accounts for a relatively small fraction of the beam weight, the material savings are limited.

The prestressing force, in Figure 4.18 also shows that the fabric formed beam is not necessarily more efficient. It requires more force than the I-beam, almost exactly that of the rectangular beam. In short, the fabric formed beam is neither more efficient in material, nor in the prestressing force required, when compared to conventional I-beams.

Figure 4.16: Normalized weight of fabric formed beam, I-Beam, and rectangular beam.

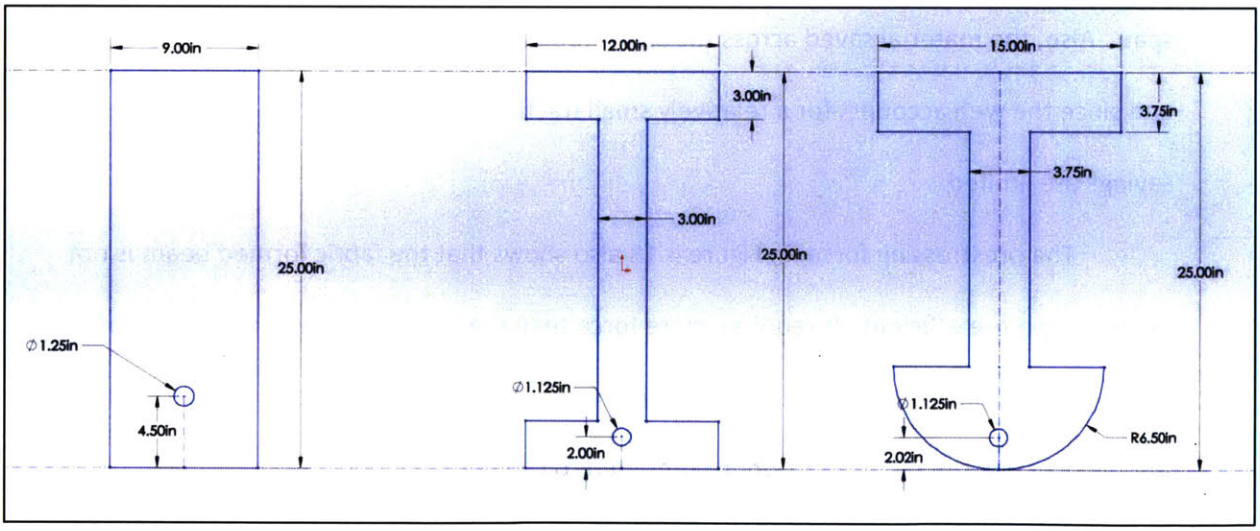

Figure 4.17: Midspan section for 35 ft. (10.7 m) beam, with section and tendon dimensions.

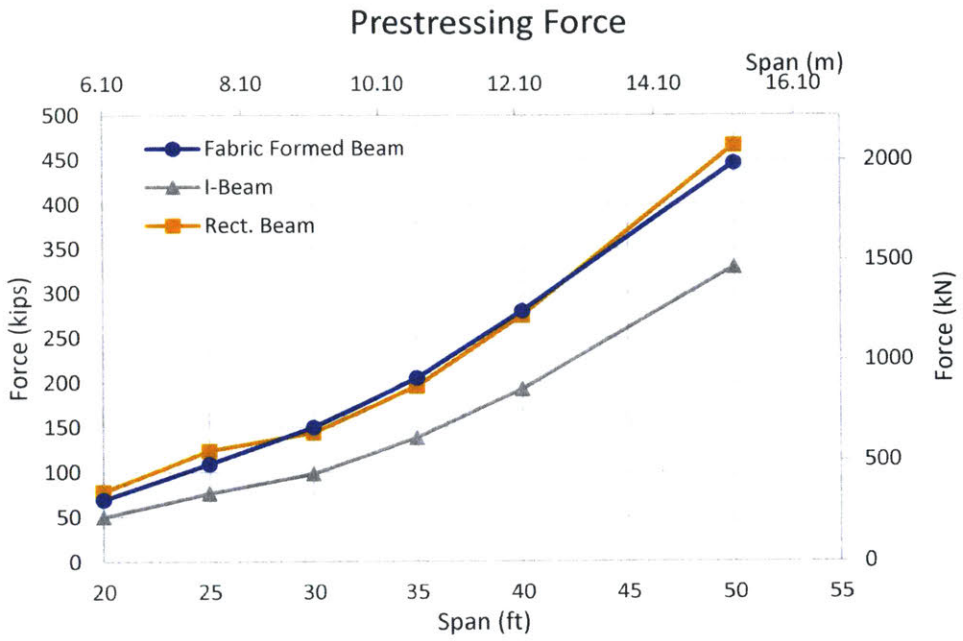

Figure 4.18: Prestressing Force for Fabric-formed beam, I-Beam, and rectangular beam

4.1 Proposed Construction

These beams would likely have to be constructed in a prestressing yard or plant. Because they are assumed to be post-tensioned, it is possible for them to be cast and then brought to the yard. However, the more controlled conditions of the yard would be advantageous to consistently creating identical casts of repeated beams. As well if one were to use higher strength concrete, then more controlled conditions are necessary to ensure the quality and consistency of the pour and material.

To create the element, a form similar to Figure 2.2 could be used, where the reinforcement shown is swapped for a duct for the post tensioning tendon. To create the keyhole shape of the beam, web-formers can be placed underneath the platforms to 'squeeze'

the fabric into the appropriate shape. Garbett et al. (2010) used this method to cast one of their beams. Figure 2.5 shows a diagram of their method.

4.2 Summary

The beams presented here all pass the strength and deflections criteria. When using the more accurate energy methods for deflection, the beam is well within serviceability criteria, and this is usually true for the approximate deflection calculated by Equation 3.18. However, even though discounting for the camber for prestressing is indeed conservative, it may prove that the initial camber may be larger than the downward deflection imposed from loading.

In general, deflection can be assumed to be non-controlling at first. A designer can likely use the simpler approximation to check deflection. The figures showing deflection calculated with Equation 3.22, while more accurate, suggest that the extra effort may not be necessary and that the approximation is sufficient.

The chosen strength of concrete seems to primarily affect the amount of material used, but does not significantly change the depth or prestress force required. At best, choosing a concrete 3x stronger, may reduce the span-to-depth ratio by just about 9%, as seen in the 30 ft (9.1 m) span of Figure 4.10. And even though the depth is reduced, the deflection is about equivalent. Figure 4.16 shows that weight per unit length can be reduced with a higher strength concrete. However, in Purnell (2013), it is found that higher strength concrete tends to have higher embodied carbon coefficients. This coupled with higher economic costs must be carefully weighed so that the tradeoff is quantified.

5. Conclusion

This work has explored the feasibility and potential efficiency of combining fabric formwork and prestressing in concrete beam design. Previous work has addressed the design and implications of fabric forms with passive reinforcement, but very little has been done with active prestressing.

By using a sectional design method discussed by Garbett et al. (2010) and Orr (2012), several prestressed beams were designed around the critical midspan section. The remainder of the beam was then determined using a parabolic form. Each section was analyzed so that the stresses under maximum hogging and sagging moments did not exceed allowable stresses. The deflections of the beams were then calculated to check for serviceability requirements.

The beams as designed in this work meet strength and serviceability criteria. The depths and prestressing forces required are certainly feasible to achieve. As well, the proposed construction process would not require a great amount of investment, as fabric formwork is inexpensive. The post-tensioning process would require a frame to hold the curved beam upright while the tendons are stressed and then the anchors transferred.

However, from an efficiency perspective, this fusion of technologies cannot be recommended for practice yet. While the material used in a fabric formed beam is less across the span, the cross section explored in this thesis is less efficient than a traditional I-beam. Both designs use less material than a traditional rectangular beam. However, the material saved across the span for the fabric-formed beam, is equivalent to the material added to make the section viable for prestressing. Aside from this, the prestressing forces required for a fabric formed beam higher than those required for the equivalent I-beam.

5.1 Future Work

There are three primary areas where future work could be focused. The first is the use of form finding methods to more accurately predict that shape made possible by a hung fabric sheet constrained between web-formers. Veenendaal et al. (2011a) has explored this initially, even considering the effects of impacto, like the web formers used by Garbett et al (2010) and the forces apparent in the fabric.

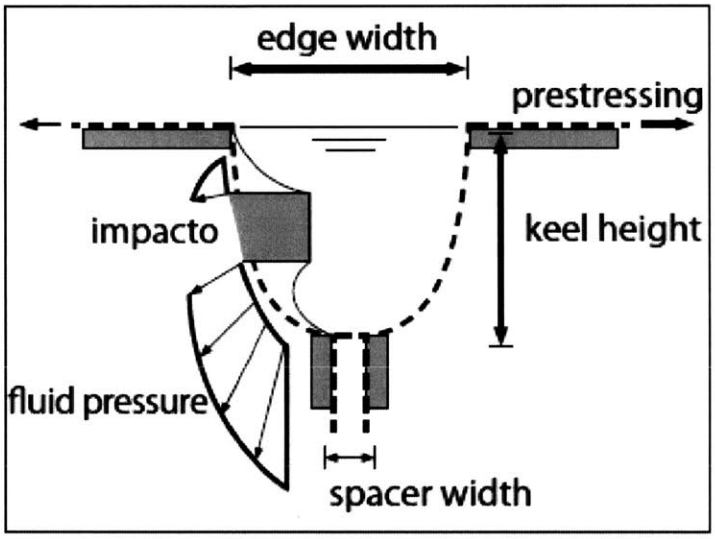

Figure 5.1: Variables in determining the form from a mold, taken from Veenendaal et al. (2011a)

The second expansion of work would be in optimizing for shear. This thesis assumed a simple ratio as the primary determinate for web thickness, however a more robust approach would minimize this thickness from the shear experienced in each section along the beam. This thesis did check for shear strength, but did not optimize web thickness for material efficiency. While this is expressed in the sectional design method by Orr (2012) and Garbett et al. (2010), prestressed shear design differs from normal reinforced concrete design, and should consider the vertical component prestressing force along with the changing strength and loading stages.

Lastly, the camber caused by the initial transfer of prestress should be determined. While excluding this for simplicity allows this papers deflections to be conservative, the resulting deformations via energy methods are very small. The net combination of initial camber plus this sagging may be a hogging deformation, and that should be checked against serviceability criteria.

5.2 Concluding Remarks

This thesis explored the performance and behavior of a prestressed fabric formed beam for a certain cross sectional geometry. Such beams are feasible and meet strength and deflection criteria. While fabric forms may help ensure material efficiency, this first approximation of using a keyhole type cross section may actually be slightly less efficient than some more traditional I-beam designs, especially when considering the prestressing force required. However, the use of prestressing combined with fabric forms is shown to be feasible and further exploration is needed.

6. References

American Concrete Institute, 2014. *Buidling Code for Structural Concrete (ACI 318-14) and Commentary.* s.l.:s.n.

Collins, M. P. & Mitchell, D., 1991. *Prestressed Concrete Structures.* Englewood Cliffs(New Jersey): Prentice-Hall, Inc..

Dywidag-Systems International, 2017. *Post Tensioning System - Ducts.* [Online] Available at: https://www.dsiamerica.com/products/post-tensioning/strand-post-tensioning-system/installation/ducts.html [Accessed May 2017].

Garbett, J., Ibell, T. J. & Darby, A. P., 2010. Optimised beam design using innovative fabric-formed concrete. *Advances in Structural Engineering,* 13(5), pp. 849-860.

Hurst, M. K., 1998. *Prestressed Concrete Design.* 2nd ed. New York: Routledge.

International Code Council, 2012. *2012 International Building Code.* s.l.:Country Club Hills, Ill:ICC.

Lin, T. Y. & Burns, N. H., 1981. *Design of Prestressed Concrete Structures.* 3rd ed. New York: John Wiley and Sons.

Menez, M. H., 2016. *Efficiency of a Fabric Formed Concrete Slab,* Cambridge: Massachusetts Institute of Technology.

Nawy, E. G., 2000. *Prestressed Concrete A Fundamental Approach.* 3rd ed. Upper Saddle River(New Jersey): Pearson Education, Inc..

Nawy, E. G., 2003. *Prestressed Concrete A Fundamental Approach.* 4th ed. Upper Saddle River(New Jersey): Pearson Education, Inc..

Orr, J. J., 2012. *Flexible formwork for concrete structures,* Bath: University of Bath.

Orr, J. J., Darby, A. P., Ibell, T. & Everden, M., 2014. Design Methods for flexibly formed concrete beams. *Proceedings of the Institution of Civil Engineers - Structures and Buildings,* 167(11), pp. 654-666.

Orr, J. J. et al., 2011. Concrete structures using fabric formwork. *The Structural Engineer,* 89(8), pp. 20-26.

PCI Industry Handbook committee, 1999. *PCI Design Handobook: Precast and Prestressed Concrete.* 5th ed. Chicago: Precast/Prestressed Concrete Institute.

Purnell, P., 2013. The carbon footprint of reinforced concrete. *Advances in cement research,* 25(6), pp. 362-368.

Sarieddine, M., 2014. *Optimal Design of Fabric Formed Concrete Beams,* Cambridge: Massachuseets Institute of Technology.

Shushkewich, K. W., 2012. Eugene Freyssinet - Invention of Prestressed Concrete and Precast Segmental Construction. *Structural Engineering International,* 22(3), pp. 415-420.

Structural Technolgies VSL, 2016. *Strand and Tendon Properties.* [Online]
Available at:
http://www.vsl.net/sites/default/files/vsl/datasheet/VSL_Datasheets_US.pdf

Veenendaal, D. & Block, P., 2012. *Computations form-finding of fabric formworks: an overview and discussion.* Bath, UK, University of Bath.

Veenendaal, D., Coenders, J., Vembersky, J. & West, M., 2011a. Design and optimization of fabric-formed beams and trusses: evolutionary algorithms and form finding. *Structural Concrete,* 12(4), pp. 241-254.

Veenendaal, D., West, M. & Block, P., 2011b. History and overview of fabric formwork: using fabrics for concrete casting. *Structural Concrete,* 12(3), pp. 164-177.

Wang, C.-K., Salmon, C. G. & Pincheira, J. A., 2007. *Reinforced Concrete Design.* 7th ed. Hoboken: John Wiley & Sons, Inc.

West, M., 2017. *The Fabric Formwork Book.* New York: Routledge.

World Business Council for Sustainable Development, 2002. *wbcsd.* [Online] Available at: https://web.archive.org/web/20070714085318/http://www.wbcsd.org/DocRoot/1IBetslPgkEie83rTa0J/cement-action-plan.pdf [Accessed March 2017].

7. Appendix

Appendix A1: Results of fabric formed beam when varying bay size

Appendix A2: Dimension of fabric formed beams when varying bay size

Appendix A3: Results of varied strength beams, where span-to-depth ratio is 20

Appendix A4: Dimensions of varied strength beams, where span-to-depth ratio is 20

Appendix A5: Results of varied strength beams, where prestress force for each span is constant

Appendix A6: Dimensions of varied strength beams, where prestress force for each span is constant

Appendix A7: Results of I-beam, rectangular beam, and fabric formed beam

Appendix A8: Dimensions of I-beam, rectangular beam, and fabric formed beam

Appendix B: Calculations of example beam, from figure 4.14

7.1 Appendix A:

Appendix A1: Results of Fabric Formed beams when varying bay size:

Strength	Span	Bay Width L/3	Depth	L/360 Limit	Estimated Deflection	Energy Deflection	P/S Force	Span Depth Ratio	Normalized Weight
	(ft)		(in)	(in)	(in)	(in)	(lbs)		(lbs/ft)
5,000 psi	20(	0.33	12	0.67	0.52	0.23	69000	20.00	37.62
5,000 psi	25	0.33	16	0.83	0.67	0.27	96000	18.75	48.04
5,000 psi	30	0.33	21	1.00	0.69	0.27	108000	17.14	65.74
5,000 psi	35	0.33	25	1.17	0.82	0.32	144000	16.80	84.24
5,000 psi	40	0.33	28	1.33	1.16	0.44	215000	17.14	93.32
5,000 psi	50	0.33	34	1.67	1.45	0.56	348000	17.65	153.04
		Bay Width L/2							
5,000 psi	20	0.5	15	0.67	0.36	0.23	66000	16.00	50.68
5,000 psi	25	0.5	19	0.83	0.51	0.31	104000	15.79	67.22
5,000 psi	30	0.5	25	1.00	0.57	0.33	131000	14.40	84.24
5,000 psi	35	0.5	30	1.17	0.70	0.40	180000	14.00	101.41
5,000 psi	40	0.5	33	1.33	0.95	0.53	260000	14.55	122.74
5,000 psi	50	0.5	39	1.67	1.19	0.69	445000	15.38	214.89
		Bay Width L/4							
5,000 psi	20	0.25	11	0.67	0.49	0.17	56000	21.82	36.70
5,000 psi	25	0.25	15	0.83	0.63	0.19	66000	20.00	43.55
5,000 psi	30	0.25	19	1.00	0.76	0.22	95000	18.95	55.10
5,000 psi	35	0.25	22	1.17	0.94	0.28	129000	19.09	71.09
5,000 psi	40	0.25	25	1.33	1.25	0.36	179000	19.20	81.02
5,000 psi	50	0.25	32	1.67	1.55	0.44	274000	18.75	121.05

Appendix A2: Mid span Dimension of Fabric Formed Beams when varying bay size:

strength	Span	Bay Width L/3	Depth (h_1)	B_{flange}	Flange thickness	Web Thickness	r_chord	Y_c.g.	e	P/S Force	Tendon Diameter
	(ft)		(in)	(in)	(in)	(in)	(in)	(in)	(in)	lbs	(in)
5,000 psi	20	0.33	15	12	3	3	5.5	7.16	6	66000	0.75
5,000 psi	25	0.33	19	14	3.5	3.5	6	8.92	8	104000	0.875
5,000 psi	30	0.33	25	15	3.75	3.75	6.5	11.9	10.5	131000	1
5,000 psi	35	0.33	30	16	4	4	7	14.5	12.25	180000	1.375
5,000 psi	40	0.33	33	18	4.5	4.5	8	16.5	13.25	260000	1.5
5,000 psi	50	0.33	39	24	6	6	11	19.4	16.25	445000	1.875
		Bay Width L/2									
5,000 psi	20	0.5	12	10	2.5	2.5	5	5.86	4	69000	0.75
5,000 psi	25	0.5	16	12	3	3	5	7.42	6	96000	0.875
5,000 psi	30	0.5	21	14	3.5	3.5	5.5	9.61	9.5	108000	1
5,000 psi	35	0.5	25	15	3.75	3.75	6.5	11.9	11	144000	1.125
5,000 psi	40	0.5	28	16	4	4	7	13.9	11	215000	1.25
5,000 psi	50	0.5	34	20	5	5	9	16.6	14.5	348000	1.75
		Bay Width L/4									
5,000 psi	20	0.25	11	10	2.5	2.5	4.5	5.14	4	55000	0.75
5,000 psi	25	0.25	15	11	2.75	2.75	5	7.20	6.5	66000	0.875
5,000 psi	30	0.25	19	12	3	3	5.5	9.27	8	95000	0.875
5,000 psi	35	0.25	22	14	3.5	3.5	6	10.4	9.5	129000	1
5,000 psi	40	0.25	25	15	3.75	3.75	6.5	12.2	10.5	179000	1.25
5,000 psi	50	0.25	32	17.5	4.375	4.375	8	15.9	13.75	274000	1.5

Appendix A1 (Metric Units)

Strength	Span	Bay Width L/3	Depth	L/360 Limit	Estimated Deflection	Energy Deflection	P/S Force	Span Depth Ratio	Normalized Weight
	(m)		(mm)	(mm)	(mm)	(mm)	(kN)		(kg/m)
34.5 Mpa	6.10	0.33	304.8	16.93	13.30	5.86	307050	20.0	112.0
34.5 Mpa	7.62	0.33	406.4	21.17	16.94	6.87	427200	18.8	143.0
34.5 Mpa	9.14	0.33	533.4	25.40	17.62	6.86	480600	17.1	195.7
34.5 Mpa	10.67	0.33	635	29.63	20.78	8.01	640800	16.8	250.7
34.5 Mpa	12.19	0.33	711.2	33.87	29.36	11.05	956750	17.1	277.8
34.5 Mpa	15.24	0.33	863.6	42.33	36.91	14.19	1548600	17.6	455.5
		Bay Width L/2							
34.5 Mpa	6.10	0.5	381	16.93	9.19	5.83	293700	16.0	150.8
34.5 Mpa	7.62	0.5	482.6	21.17	12.88	7.84	462800	15.8	200.1
34.5 Mpa	9.14	0.5	635	25.40	14.42	8.34	582950	14.4	250.7
34.5 Mpa	10.67	0.5	762	29.63	17.82	10.08	801000	14.0	301.8
34.5 Mpa	12.19	0.5	838.2	33.87	24.04	13.50	1157000	14.5	365.3
34.5 Mpa	15.24	0.5	990.6	42.33	30.34	17.61	1980250	15.4	639.6
		Bay Width L/4							
34.5 Mpa	6.10	0.25	279.4	16.93	13.28	4.42	244750	21.8	99.0
34.5 Mpa	7.62	0.25	381	21.17	16.06	4.94	293700	20.0	129.6
34.5 Mpa	9.14	0.25	482.6	25.40	19.30	5.70	422750	18.9	164.0
34.5 Mpa	10.67	0.25	558.8	29.63	23.97	7.02	574050	19.1	211.6
34.5 Mpa	12.19	0.25	635	33.87	31.76	9.09	796550	19.2	241.1
34.5 Mpa	15.24	0.25	812.8	42.33	39.42	11.19	1219300	18.8	360.3

Appendix A2 (Metric Units)

strength	Span	Bay Width L/3	Depth (h_1)	B_{flange}	Flange thickness	Web Thickness	r_chord	Y_c.g.	e	P/S Force	Tendon Diameter
	(m)		(mm)	(mm)	(mm)	(mm)	(mm)	(mm)	(mm)	(kN)	(mm)
34.5 Mpa	6.096	0.33	381	305	76	76	140	182	152	293700	19
34.5 Mpa	7.62	0.33	483	356	89	89	152	227	203	462800	22
34.5 Mpa	9.144	0.33	635	381	95	95	165	304	267	582950	25
34.5 Mpa	10.668	0.33	762	406	102	102	178	369	311	801000	35
34.5 Mpa	12.192	0.33	838	457	114	114	203	420	337	1157000	38
34.5 Mpa	15.24	0.33	991	610	152	152	279	494	413	1980250	48
		Bay Width L/2									
34.5 Mpa	6.096	0.5	305	254	64	64	127	149	102	307050	19
34.5 Mpa	7.62	0.5	406	305	76	76	127	189	152	427200	22
34.5 Mpa	9.144	0.5	533	356	89	89	140	244	241	480600	25
34.5 Mpa	10.668	0.5	635	381	95	95	165	304	279	640800	29
34.5 Mpa	12.192	0.5	711	406	102	102	178	354	279	956750	32
34.5 Mpa	15.24	0.5	864	508	127	127	229	424	368	1548600	44
		Bay Width L/4									
34.5 Mpa	6.096	0.25	279	254	64	64	114	131	102	244750	19
34.5 Mpa	7.62	0.25	381	279	70	70	127	183	165	293700	22
34.5 Mpa	9.144	0.25	483	305	76	76	140	235	203	422750	22
34.5 Mpa	10.668	0.25	559	356	89	89	152	266	241	574050	25
34.5 Mpa	12.192	0.25	635	381	95	95	165	311	267	796550	32
34.5 Mpa	15.24	0.25	813	445	111	111	203	405	349	1219300	38

Appendix A3: Results of fabric formed beams when varying concrete strength, and constraining Span/depth ratio to 20

Strength	Span	Bay Ratio L/3	Depth	L/360 Limit	Approximate Deflection	Energy Deflection	P/S Force	Span Depth Ratio	Normalized Weight
	(ft)		(in)	(in)	(in)	(in)	(lbs)		(lbs/ft)
5,000 psi	20	0.33	12	0.67	0.52	0.23	69000	20	37.62
5,000 psi	25	0.33	15	0.83	0.65	0.28	109000	20	58.34
5,000 psi	30	0.33	18	1.00	0.78	0.34	150000	20	83.73
5,000 psi	35	0.33	21	1.17	0.68	0.27	205000	20	105.63
5,000 psi	40	0.33	24	1.33	1.12	0.48	280000	20	136.77
5,000 psi	50	0.33	30	1.67	1.23	0.48	446000	20	183.26
10,000 psi	20	0.33	12	0.67	0.62	0.24	65000	20	23.14
10,000 psi	25	0.33	15	0.83	0.82	0.32	102000	20	33.94
10,000 psi	30	0.33	18	1.00	0.96	0.38	142000	20	50.25
10,000 psi	35	0.33	21	1.17	1.10	0.43	195000	20	69.80
10,000 psi	40	0.33	24	1.33	1.44	0.56	268000	20	78.43
10,000 psi	50	0.33	30	1.67	1.96	0.75	431000	20	112.22
15,000 psi	20	0.33	12	0.67	0.56	0.22	56000	20	20.85
15,000 psi	25	0.33	15	0.83	0.88	0.33	99000	20	25.35
15,000 psi	30	0.33	18	1.00	0.98	0.37	139000	20	40.24
15,000 psi	35	0.33	21	1.17	1.01	0.39	186000	20	61.42
15,000 psi	40	0.33	24	1.33	1.41	0.53	255000	20	65.01
15,000 psi	50	0.33	30	1.67	1.95	0.73	420000	20	91.14

Appendix A4: Dimensions of fabric formed beams when varying concrete strength, and constraining Span/depth ratio to 20

strength	Span	bay ratio	Depth (h_1)	B_{flange}	Flange thickness	Web Thickness	r_chord	Y_c.g.	e	P/S Force	Tendon Diameter
	(ft)		(in)	(in)	(in)	(in)	(in)	(in)	(in)	lbs	(in)
5,000 psi	20	0.33	12	10	2.5	2.5	5	5.86	4	69000	0.75
5,000 psi	25	0.33	15	13	3.25	3.25	6	7.11	5.25	109000	1
5,000 psi	30	0.33	18	16	4	4	7	8.36	7	150000	1.125
5,000 psi	35	0.33	21	19	4.75	4.75	8	9.61	8.75	205000	1.25
5,000 psi	40	0.33	24	20	5	5	9	11.3	9.5	280000	1.5
5,000 psi	50	0.33	30	24	6	6	11.5	14.5	12	446000	1.75
10,000 psi	20	0.33	12	8	2	2	3.5	5.72	4.25	65000	0.75
10,000 psi	25	0.33	15	10	2.5	2.5	4	6.91	5.5	102000	1
10,000 psi	30	0.33	18	12	3	3	5	8.43	7	142000	1.125
10,000 psi	35	0.33	21	14	3.5	3.5	6	9.94	8.25	195000	1.25
10,000 psi	40	0.33	24	15	3.75	3.75	6	11.1	9.25	268000	1.5
10,000 psi	50	0.33	30	17	4.25	4.25	7.5	14.5	11.25	431000	1.75
15,000 psi	20	0.33	12	8	2	2	3	5.39	5	56000	0.75
15,000 psi	25	0.33	15	8	2	2	3.5	7.26	5.25	99000	1
15,000 psi	30	0.33	18	11	2.75	2.75	4	8.05	7.25	139000	1.125
15,000 psi	35	0.33	21	13	3.25	3.25	5.5	9.9	8.25	186000	1.25
15,000 psi	40	0.33	24	13	3.25	3.25	5.5	11.4	9.25	255000	1.5
15,000 psi	50	0.33	30	15	3.75	3.75	6.5	14.5	11.25	420000	1.75

Appendix A3 (Metric Units)

Strength	Span	Bay Ratio L/3	Depth	L/360 Limit	Estimated Deflection	Energy Deflection	P/S Force	Span Depth Ratio	Normalized Weight
34.5 Mpa	6.10	0.33	304.8	16.93	13.30	5.86	307050	20	112.0
34.5 Mpa	7.62	0.33	381.0	21.17	16.51	7.22	485050	20	173.6
34.5 Mpa	9.14	0.33	457.2	25.40	19.77	8.61	667500	20	249.2
34.5 Mpa	10.67	0.33	533.4	29.63	17.21	6.77	912250	20	314.4
34.5 Mpa	12.19	0.33	609.6	33.87	28.48	12.18	1246000	20	407.1
34.5 Mpa	15.24	0.33	762.0	42.33	31.29	12.26	1984700	20	545.4
69 Mpa	6.10	0.33	304.8	16.93	15.68	6.21	289250	20	68.9
69 Mpa	7.62	0.33	381.0	21.17	20.82	8.13	453900	20	101.0
69 Mpa	9.14	0.33	457.2	25.40	24.30	9.55	631900	20	149.6
69 Mpa	10.67	0.33	533.4	29.63	27.82	10.98	867750	20	207.7
69 Mpa	12.19	0.33	609.6	33.87	36.67	14.11	1192600	20	233.4
69 Mpa	15.24	0.33	762.0	42.33	49.71	18.99	1917950	20	334.0
103.4 Mpa	6.10	0.33	304.8	16.93	14.22	5.50	249200	20	62.1
103.4 Mpa	7.62	0.33	381.0	21.17	22.35	8.43	440550	20	75.5
103.4 Mpa	9.14	0.33	457.2	25.40	24.79	9.37	618550	20	119.8
103.4 Mpa	10.67	0.33	533.4	29.63	25.59	9.90	827700	20	182.8
103.4 Mpa	12.19	0.33	609.6	33.87	35.72	13.45	1134750	20	193.5
103.4 Mpa	15.24	0.33	762.0	42.33	49.55	18.44	1869000	20	271.3

Appendix A4 (Metric Units)

strength	Span	bay ratio	Depth (h_1)	B_{flange}	Flange thickness	Web Thickness	r_chord	Y_c.g.	e	P/S Force	Tendon Diameter
	(m)		(mm)	(mm)	(mm)	(mm)	(mm)	(mm)	(mm)	(kN)	(mm)
34.5 Mpa	6.096	0.33	305	254	64	64	127	149	102	307050	19
34.5 Mpa	7.62	0.33	381	330	83	83	152	181	133	485050	25
34.5 Mpa	9.144	0.33	457	406	102	102	178	212	178	667500	29
34.5 Mpa	10.668	0.33	533	483	121	121	203	244	222	912250	32
34.5 Mpa	12.192	0.33	610	508	127	127	229	288	241	1246000	38
34.5 Mpa	15.24	0.33	762	610	152	152	292	369	305	1984700	44
69 Mpa	6.096	0.33	305	203	51	51	89	146	108	289250	19
69 Mpa	7.62	0.33	381	254	64	64	102	176	140	453900	25
69 Mpa	9.144	0.33	457	305	76	76	127	214	178	631900	29
69 Mpa	10.668	0.33	533	356	89	89	152	253	210	867750	32
69 Mpa	12.192	0.33	610	381	95	95	152	282	235	1192600	38
69 Mpa	15.24	0.33	762	432	108	108	191	369	286	1917950	44
103.4 Mpa	6.096	0.33	305	203	51	51	76	137	127	249200	19
103.4 Mpa	7.62	0.33	381	203	51	51	89	185	133	440550	25
103.4 Mpa	9.144	0.33	457	279	70	70	102	205	184	618550	29
103.4 Mpa	10.668	0.33	533	330	83	83	140	253	210	827700	32
103.4 Mpa	12.192	0.33	610	330	83	83	140	291	235	1134750	38
103.4 Mpa	15.24	0.33	762	381	95	95	165	369	286	1869000	44

Appendix A5: Results of fabric formed beams when varying concrete strength, and constraining prestress force

Strength	Span	Bay Ratio L/3	Depth	L/360 Limit	Approximate Deflection	Energy Deflection	P/S Force	Span Depth Ratio	Normalized Weight
	(ft)		(in)	(in)	(in)	(in)	(lbs)		(lbs/ft)
5,000 psi	20	0.33	12	0.67	0.52	0.23	69000	20.00	37.62
5,000 psi	25	0.33	16	0.83	0.67	0.27	96000	18.75	48.04
5,000 psi	30	0.33	21	1.00	0.73	0.28	110000	17.14	62.74
5,000 psi	35	0.33	25	1.17	0.88	0.33	147000	16.80	79.41
5,000 psi	40	0.33	28	1.33	1.16	0.44	215000	17.14	93.32
5,000 psi	50	0.33	34	1.67	1.45	0.56	348000	17.65	153.04
10,000 psi	20	0.33	12	0.67	0.56	0.22	69000	20.00	25.75
10,000 psi	25	0.33	15.5	0.83	0.76	0.30	96000	19.35	36.95
10,000 psi	30	0.33	20	1.00	0.71	0.27	110000	18.00	54.47
10,000 psi	35	0.33	24	1.17	0.86	0.32	147000	17.50	67.28
10,000 psi	40	0.33	27	1.33	1.14	0.43	215000	17.78	77.53
10,000 psi	50	0.33	33	1.67	1.42	0.54	348000	18.18	137.29
15,000 psi	20	0.33	12	0.67	0.67	0.25	69000	20.00	17.70
15,000 psi	25	0.33	15	0.83	0.76	0.29	96000	20.00	29.76
15,000 psi	30	0.33	19	1.00	0.73	0.28	110000	18.95	48.02
15,000 psi	35	0.33	23	1.17	0.86	0.32	147000	18.26	60.11
15,000 psi	40	0.33	26	1.33	1.12	0.41	215000	18.46	69.77
15,000 psi	50	0.33	32	1.67	1.50	0.57	348000	18.75	103.00

Appendix A6: Dimensions of fabric formed beams when varying concrete strength, and constraining prestress force

strength	Span	bay ratio	Depth (h_1)	B_{flange}	Flange thickness	Web Thickness	r_chord	Y_c.g.	e	P/S Force	Tendon Diameter
	(ft)		(in)	(in)	(in)	(in)	(in)	(in)	(in)	lbs	(in)
5,000 psi	20	0.33	12	10	2.5	2.5	5	5.86	4	69000	0.75
5,000 psi	25	0.33	16	12	3	3	5	7.43	6	96000	0.875
5,000 psi	30	0.33	21	14	3.5	3.5	5.5	9.87	9	110000	1
5,000 psi	35	0.33	25	15	3.75	3.75	6.5	12.4	10.5	147000	1.125
5,000 psi	40	0.33	28	16	4	4	7	14	11	215000	1.25
5,000 psi	50	0.33	34	20	5	5	9	16.7	14.5	348000	1.75
10,000 psi	20	0.33	12	9	2.25	2.25	3	5.11	4.5	69000	0.75
10,000 psi	25	0.33	15.5	10	2.5	2.5	4	7.17	6	96000	0.875
10,000 psi	30	0.33	20	12.5	3.125	3.125	5	9.27	9	110000	1
10,000 psi	35	0.33	24	13.5	3.375	3.375	5.5	11.3	10.75	147000	1.125
10,000 psi	40	0.33	27	14	3.5	3.5	6	13	11	215000	1.25
10,000 psi	50	0.33	33	20	5	5	7	14.7	15	348000	1.75
15,000 psi	20	0.33	12	7.5	1.875	1.875	2.5	5.19	4.5	69000	0.75
15,000 psi	25	0.33	15	9.5	2.375	2.375	3.5	6.73	6	96000	0.875
15,000 psi	30	0.33	19	12	3	3	4.5	8.58	8.75	110000	1
15,000 psi	35	0.33	23	13	3.25	3.25	5	10.6	10.5	147000	1.125
15,000 psi	40	0.33	26	13.5	3.375	3.375	5.5	12.3	11	215000	1.25
15,000 psi	50	0.33	32	14.5	3.625	3.625	7	15.5	14.5	348000	1.75

Appendix A5 (Metric Units)

Strength	Span	Bay Ratio L/3	Depth	L/360 Limit	Estimated Deflection	Energy Deflection	P/S Force	Span Depth Ratio	Normalized Weight
	(m)		(mm)	(mm)	(mm)	(mm)	(kN)	(mm)	(mm)
34.5 Mpa	6.10	0.33	304.8	16.93	13.30	5.86	307050	20.0	112.0
34.5 Mpa	7.62	0.33	406.4	21.17	16.94	6.87	427200	18.8	143.0
34.5 Mpa	9.14	0.33	533.4	25.40	18.45	7.09	489500	17.1	186.7
34.5 Mpa	10.67	0.33	635	29.63	22.28	8.45	654150	16.8	236.4
34.5 Mpa	12.19	0.33	711.2	33.87	29.36	11.05	956750	17.1	277.8
34.5 Mpa	15.24	0.33	863.6	42.33	36.91	14.19	1548600	17.6	455.5
69 Mpa	6.10	0.33	304.8	16.93	14.25	5.71	302600	20.0	76.6
69 Mpa	7.62	0.33	393.7	21.17	19.24	7.66	427200	19.4	110.0
69 Mpa	9.14	0.33	508	25.40	18.05	6.94	489500	18.0	162.1
69 Mpa	10.67	0.33	609.6	29.63	21.74	8.21	654150	17.5	200.2
69 Mpa	12.19	0.33	685.8	33.87	28.91	10.81	956750	17.8	230.8
69 Mpa	15.24	0.33	838.2	42.33	35.95	13.77	1548600	18.2	408.6
103.4 Mpa	6.10	0.33	304.8	16.93	16.97	6.37	302600	20.0	52.7
103.4 Mpa	7.62	0.33	381	21.17	19.41	7.40	427200	20.0	88.6
103.4 Mpa	9.14	0.33	482.6	25.40	18.61	7.11	489500	18.9	142.9
103.4 Mpa	10.67	0.33	584.2	29.63	21.72	8.15	654150	18.3	178.9
103.4 Mpa	12.19	0.33	660.4	33.87	28.33	10.54	956750	18.5	207.6
103.4 Mpa	15.24	0.33	812.8	42.33	38.07	14.38	1548600	18.8	306.6

Appendix A6 (Metric Units)

strength	Span	bay ratio	Depth (h_1)	B_{flange}	Flange thickness	Web Thickness	r_chord	Y_c.g.	e	P/S Force	Tendon Diameter
	(m)		(mm)	(mm)	(mm)	(mm)	(mm)	(mm)	(mm)	(kN)	(mm)
34.5 Mpa	6.096	0.33	305	254	64	64	127	149	102	307050	19
34.5 Mpa	7.62	0.33	406	305	76	76	127	189	152	427200	22
34.5 Mpa	9.144	0.33	533	356	89	89	140	251	229	489500	25
34.5 Mpa	10.668	0.33	635	381	95	95	165	315	267	654150	29
34.5 Mpa	12.192	0.33	711	406	102	102	178	354	279	956750	32
34.5 Mpa	15.24	0.33	864	508	127	127	229	424	368	1548600	44
69 Mpa	6.096	0.33	305	229	57	57	76	130	114	307050	19
69 Mpa	7.62	0.33	394	254	64	64	102	182	152	427200	22
69 Mpa	9.144	0.33	508	318	79	79	127	235	229	489500	25
69 Mpa	10.668	0.33	610	343	86	86	140	286	273	654150	29
69 Mpa	12.192	0.33	686	356	89	89	152	330	279	956750	32
69 Mpa	15.24	0.33	838	508	127	127	178	373	381	1548600	44
103.4 Mpa	6.096	0.33	305	191	48	48	64	132	114	307050	19
103.4 Mpa	7.62	0.33	381	241	60	60	89	171	152	427200	22
103.4 Mpa	9.144	0.33	483	305	76	76	114	218	222	489500	25
103.4 Mpa	10.668	0.33	584	330	83	83	127	268	267	654150	29
103.4 Mpa	12.192	0.33	660	343	86	86	140	312	279	956750	32
103.4 Mpa	15.24	0.33	813	368	92	92	178	395	368	1548600	44

Appendix A7: Results of rectangular beam and I-beam with 5,000 psi concrete and constrained to same depth as fabric formed beam, with equivalent fabric formed beam for reference:

Strength	Span	Bay Ratio L/3	Depth	L/360 Limit	Estimated Deflection	Energy Deflection	P/S Force	Span Depth Ratio	Normalized Weight
	(ft)		(in)	(in)	(in)	(in)	(lbs)		(lbs/ft)
I-Beam									
5,000 psi	20	0.3333333	12	0.67	0.39		52000	20.00	59.77
5,000 psi	25	0.3333333	16	0.83	0.48		80000	18.75	80.73
5,000 psi	30	0.3333333	21	1.00	0.52		102000	17.14	107.42
5,000 psi	35	0.3333333	25	1.17	0.64		143000	16.80	134.38
5,000 psi	40	0.3333333	28	1.33	0.75		192000	17.14	178.65
5,000 psi	50	0.3333333	34	1.67	0.96		329000	17.65	285.94
Rectangular Beam									
5,000 psi	20	0.3333333	12	0.67	0.35		78000	20.00	100.00
5,000 psi	25	0.3333333	16	0.83	0.46		124000	18.75	133.33
5,000 psi	30	0.3333333	21	1.00	0.50		156000	17.14	175.00
5,000 psi	35	0.3333333	25	1.17	0.57		214000	16.80	234.38
5,000 psi	40	0.3333333	28	1.33	0.65		275000	17.14	320.83
5,000 psi	50	0.3333333	34	1.67	0.87		466000	17.65	495.83
Fabric Formed Beam									
5,000 psi	20	0.3333333	12	0.67	0.52	0.23	69000	20.00	75.24
5,000 psi	25	0.3333333	16	0.83	0.67	0.27	96000	18.75	96.09
5,000 psi	30	0.3333333	21	1.00	0.73	0.28	110000	17.14	125.47
5,000 psi	35	0.3333333	25	1.17	0.88	0.33	147000	16.80	158.82
5,000 psi	40	0.3333333	28	1.33	1.16	0.44	215000	17.14	186.64
5,000 psi	50	0.3333333	34	1.67	1.45	0.56	348000	17.65	306.08

*energy methods deflection not calculated since the approximation equation assumes a uniform section, which the I-beam and rectangular beam are

Appendix A8: Dimensions of rectangular beam and I-beam with 5,000 psi concrete and constrained to same depth as fabric formed beam, with equivalent fabric formed beam for reference:

strength	Span	bay ratio	Depth (h_1)	B_{flange}	Flange thickness	Web Thickness	r_chord	Y_c.g.	e	P/S Force	Tendon Diameter
	(ft)		(in)	(in)	(in)	(in)	(in)	(in)	(in)	lbs	(in)
I Beam											
5,000 psi	20	0.33	12	9	2.25	2.25		6	5	52000	0.75
5,000 psi	25	0.33	16	10	2.5	2.5		8	6.5	80000	0.875
5,000 psi	30	0.33	21	11	2.75	2.75		10.5	9	102000	1
5,000 psi	35	0.33	25	12	3	3		12.5	10.5	143000	1.125
5,000 psi	40	0.33	28	14	3.5	3.5		14	12	192000	1.25
5,000 psi	50	0.33	34	18	4.5	4.5		17	14	329000	1.75
Rectangular Beam											
5,000 psi	20	0.33	12	8				6	3.5	78000	0.875
5,000 psi	25	0.33	16	8				8	4.5	124000	1
5,000 psi	30	0.33	21	8				10.5	6.5	156000	1.125
5,000 psi	35	0.33	25	9				12.5	8	214000	1.25
5,000 psi	40	0.33	28	11				14	9.5	275000	1.5
5,000 psi	50	0.33	34	14				17	12	466000	1.875
Fabric Formed Beam											
5,000 psi	20	0.33	12	10	2.5	2.5	5	5.86	4	69000	0.75
5,000 psi	25	0.33	16	12	3	3	5	7.43	6	96000	0.875
5,000 psi	30	0.33	21	14	3.5	3.5	5.5	9.87	9	110000	1
5,000 psi	35	0.33	25	15	3.75	3.75	6.5	12.4	10.5	147000	1.125
5,000 psi	40	0.33	28	16	4	4	7	14	11	215000	1.25
5,000 psi	50	0.33	34	20	5	5	9	16.7	14.5	348000	1.75

Appendix A7 (Metric Units)

Strength	Span	Bay Ratio L/3	Depth	L/360 Limit	Estimated Deflection	Energy Deflection	P/S Force	Span Depth Ratio	Normalized Weight
II-Beam	(m)		(mm)	(mm)	(mm)	(mm)	(kN)		(kg/m)
34.5 Mpa	6.10	0.33	304.8	16.9	9.8		231400	20.00	88.9
34.5 Mpa	7.62	0.33	406.4	21.2	12.3		356000	18.75	120.1
34.5 Mpa	9.14	0.33	533.4	25.4	13.3		453900	17.14	159.9
34.5 Mpa	10.67	0.33	635	29.6	16.3		636350	16.80	200.0
34.5 Mpa	12.19	0.33	711.2	33.9	19.0		854400	17.14	265.9
34.5 Mpa	15.24	0.33	863.6	42.3	24.5		1464050	17.65	425.5
Rectangular Beam									
34.5 Mpa	6.10	0.33	304.8	16.9	9.0		347100	20.00	148.8
34.5 Mpa	7.62	0.33	406.4	21.2	11.6		551800	18.75	198.4
34.5 Mpa	9.14	0.33	533.4	25.4	12.8		694200	17.14	260.4
34.5 Mpa	10.67	0.33	635	29.6	14.5		952300	16.80	348.8
34.5 Mpa	12.19	0.33	711.2	33.9	16.5		1223750	17.14	477.5
34.5 Mpa	15.24	0.33	863.6	42.3	22.1		2073700	17.65	737.9
Fabric Formed Beam									
34.5 Mpa	6.10	0.33	304.8	16.9	13.3	5.9	307050	20.00	112.0
34.5 Mpa	7.62	0.33	406.4	21.2	16.9	6.9	427200	18.75	143.0
34.5 Mpa	9.14	0.33	533.4	25.4	18.5	7.1	489500	17.14	186.7
34.5 Mpa	10.67	0.33	635	29.6	22.3	8.4	654150	16.80	236.4
34.5 Mpa	12.19	0.33	711.2	33.9	29.4	11.1	956750	17.14	277.8
34.5 Mpa	15.24	0.33	863.6	42.3	36.9	14.2	1548600	17.65	455.5

Appendix A8 (Metric Units)

strength	Span	bay ratio	Depth (h_1)	B_{flange}	Flange thickness	Web Thickness	r_chord	Y_c.g.	e	P/S Force	Tendon Diameter
	(m)		(mm)	(mm)	(mm)	(mm)	(mm)	(mm)	(mm)	(kN)	(mm)
I Beam											
34.5 Mpa	6.096	0.33	305	229	57	57		152	127	231400	19
34.5 Mpa	7.62	0.33	406	254	64	64		203	165	356000	22
34.5 Mpa	9.144	0.33	533	279	70	70		267	229	453900	25
34.5 Mpa	10.668	0.33	635	305	76	76		318	267	636350	29
34.5 Mpa	12.192	0.33	711	356	89	89		356	305	854400	32
34.5 Mpa	15.24	0.33	864	457	114	114		432	356	1464050	44
Rectangular Beam											
34.5 Mpa	6.096	0.33	305	203				152	89	347100	22
34.5 Mpa	7.62	0.33	406	203				203	114	551800	25
34.5 Mpa	9.144	0.33	533	203				267	165	694200	29
34.5 Mpa	10.668	0.33	635	229				318	203	952300	32
34.5 Mpa	12.192	0.33	711	279				356	241	1223750	38
34.5 Mpa	15.24	0.33	864	356				432	305	2073700	48
Fabric Formed Beam											
34.5 Mpa	6.096	0.33	305	254	64	64	127	149	102	307050	19
34.5 Mpa	7.62	0.33	406	305	76	76	127	189	152	427200	22
34.5 Mpa	9.144	0.33	533	356	89	89	140	251	229	489500	25
34.5 Mpa	10.668	0.33	635	381	95	95	165	315	267	654150	29
34.5 Mpa	12.192	0.33	711	406	102	102	178	354	279	956750	32
34.5 Mpa	15.24	0.33	864	508	127	127	229	424	368	1548600	44

Appendix B1: Calculations for an example beam:

$Span = 35\,ft$

$Bay\ width;\ L/3 = 11.67\,ft$

**span-to-depth ratio constrained to 20. So depth is 21 in.

Concrete Properties:

$Density = 150\,pcf$
$f'_c = 10{,}000\,psi$
$E_c = 33 * (150\,pcf)^{1.5} * \sqrt{10{,}000psi} = 6{,}062{,}487\,psi$

Allowable Stresses:

Strength at Transfer:

$$f'_{ci} = .75 * f'_c = (.75) * (10{,}000\,psi) = 7{,}500\,psi$$

Allowable compressive stress

$$f_{ci} = .6 * f'_c = (.6) * (7{,}500\,psi) = 4{,}500\,psi$$

Allowable tensile stress

$$f_{ti} = 6 * \sqrt{f'_{ci}} = 6 * \sqrt{7{,}500\,psi} = 519.6\,psi$$

Strength at 28 days:

Allowable compressive stress

$$f_c = .6 * f'_c = .6 * (10{,}000\,psi) = 6{,}000\,psi$$

Allowable tensile stress

$$f_t = 12 * \sqrt{f'_c} = 12 * \sqrt{10{,}000\,psi} = 1{,}200\,psi$$

Steel Properties:

$Tensile\ strength = 270{,}000\,psi$

Maximum Allowable tensile stress

$$= .7 * strength = .7 * (270{,}000\,psi) = 189{,}000\,psi$$

Prestress loss ratio γ = 82%

Loads:

$Live\ Load = 80\,psf$

⇨ $(80\,psf) * (11.67\,ft) = 933\,plf$

Service Dead Load from 3 inch deck:

$$(150\,pcf) * (3in * \tfrac{1\,ft}{12\,in}) = 37.5\,psf$$

⇨ $(37.5\,psf) * (11.67ft) = 437.5\,plf$

$Assume\ self\ weight = 125\,plf$

Moments

$$M_{SW} = \frac{wl^2}{8} = \frac{(125\,plf) * (35ft)^2}{8} = 229{,}687.5\ lb - in$$
$$M_{SD} = \frac{wl^2}{8} = \frac{(437.5\,plf) * (35ft)^2}{8} = 803{,}906.25\ lb - in$$
$$M_{LL} = \frac{wl^2}{8} = \frac{(933\,plf) * (35ft)^2}{8} = 1{,}715{,}000\ lb - in$$

Minimum Section moduli

$$S^{top} \geq \frac{(1-\gamma) * M_{SW} + M_{SD} + M_{LL}}{(\gamma * f_{ti} - f_c)} = 398.4\ in^3$$

$$S_{bottom} \geq \frac{(1-\gamma) * M_{SW} + M_{SD} + M_{LL}}{(f_t - \gamma * f_{ci})} = 523.6\ in^3$$

Sizing of the Midspan

$Depth = h_1 = 21\ in$

$B_{flange} = 14\ in$

⇨ $t_{flange} = b_{web} = (.25) * 14\ in = 3.5\ in$

$r_{chord} = 6\ in$

Geometric Properties:

$$Area = (B_{flange} * t_{flange}) + (h_1 - r_{chord} - t_{flange}) + (.5 * \pi * {r_{chord}}^2)$$
$$= 145.8\ in^2$$

$$Weight = (145.8\ in^2) * \frac{(150\,pcf)}{\left(144\ {}^{in^2}/_{ft^2}\right)} = 151.8\,plf$$

***Weight assumption was off*
Redo self-weight assumption...

New Self Weight Moment:

$$M_{SW} = \frac{wl^2}{8} = \frac{(151\,plf) * (35ft)^2}{8} = 277{,}462.5\ lb - in$$

New Minimum Section moduli:

$S^{top} \geq 399.8\ in^3$
$S_{bottom} \geq 525.3\ in^3$

Good... Now continue with Geometric Properties...

$y_{c.g.} = 9.94\ in\ from\ the\ top$
$I_{xx} = 7{,}213.6\ in^4\ about\ the\ centroid$
$r^2 = square\ of\ radius\ of\ gyration = \frac{I_{xx}}{Area} = 49\ in^2$
$c^t = 9.94\ in$
$S^{top} = \frac{I_{xx}}{c^t} = 725.2\ in^3$ ... Larger than minimum, Good!
$c_b = (21\ in - 9.94\ in) = 11.05\ in$
$S_{bottom} = \frac{I_{xx}}{c_b} = 652.6\ in^3$ ... Larger than minimum, Good!

Design Prestress

Choose Pi and e
$P_i = 195{,}000\ lbs$
$P_e = \gamma * P_i = (.82) * (150{,}000lbs) = 159{,}900\ lbs$
$e = 8.25\ in$

At Transfer:

$$f^{top} = \frac{-P_i}{A_c} + \left(\frac{P_i * e * c_t}{I_{xx}}\right) + \frac{-M_{SelfWeight}}{S^{top}} = \frac{-195{,}000}{145.8} + \frac{195{,}000 * 8.25 * 9.94}{7213.6} + \frac{-277{,}462}{752.2}$$

$= 498\ psi\ in\ tension, within\ allowable.\ Good!$

$$f_{bottom} = \frac{-P_i}{A_c} + \left(\frac{-P_i * e * c_b}{I_{xx}}\right) + \frac{M_{SelfWeight}}{S_{bottom}} = \frac{-195{,}000}{145.8} + \frac{-195{,}000 * 8.25 * 11.05}{7213.6} + \frac{277{,}462}{652.6}$$

$= 3377.3\ psi\ in\ compression, within\ allowable.\ Good!$

During Transport:

$$f^{top} = \frac{-P_e}{A_c} + \left(\frac{P_e * e * c_t}{I_{xx}}\right) + \frac{-M_{SelfWeight}}{S^{top}} = \frac{-159{,}900}{145.8} + \left(\frac{159{,}900 * 8.25 * 9.94}{7213.6}\right) + \frac{-277{,}462}{752.2}$$

$= 339\ psi\ in\ tension, within\ allowable.\ Good!$

$$f_{bottom} = \frac{-P_e}{A_c} + \left(\frac{-P_e * e * c_b}{I_{xx}}\right) + \frac{M_{SelfWeight}}{S_{bottom}} = \frac{-159{,}900}{145.8} + \left(\frac{-159{,}900 * 8.25 * 11.054}{7213.6}\right) + \frac{277{,}462}{652.6}$$

$= 2692.85\ psi\ in\ compression, within\ allowable.\ Good!$

In Service:

$$f^{top} = \frac{-P_e}{A_c} + \left(\frac{P_e * e * c_t}{I_{xx}}\right) + \frac{-M_{total}}{S^{top}} = \frac{-159{,}900}{145.8} + \left(\frac{159{,}900 * 8.25 * 11.054}{7213.6}\right) + \frac{-2{,}796{,}369}{752.2}$$

$$= 3133.7\ psi\ in\ compression, within\ allowable.\ Good!$$

$$f_{bottom} = \frac{-P_e}{A_c} + \left(\frac{-P_e * e * c_b}{I_{xx}}\right) + \frac{M_{total}}{S_{bottom}} = \frac{-159{,}900}{145.8} + \left(\frac{-159{,}900 * 8.25 * 11.054}{7213.6}\right) + \frac{-2{,}796{,}369}{652.6}$$

$$= 1166.67\ psi\ in\ tension, within\ allowable\ stress.\ Good!$$

Tendon Diameter:

$$Allowable\ steel\ stress\ = 189{,}000\ psi.$$

$$\frac{P_i}{189{,}000\ pi} = minimum\ area\ of\ steel\ tendon\ = 1.03\ in^2$$

$$\sqrt{\frac{1.03\ in^2 * 4}{\pi}} = minimum\ diameter = 1.146\ in$$

Choose *1.25 in* diameter tendon

Check concrete cover...

$$Distance\ to\ bottom\ fiber\ = h_1 - y_{c.g.} - e\ = (21\ in - 9.94\ in - 8.25\ in\ ) = 2.8\ in$$

$$Concrete\ cover\ = 2.8\ in - \frac{1.25\ in}{2}\ = 2.177\ in$$

...larger than 5/8' and/or the tendon diameter, good!